Supplementary Information

Synthesis of Annulated Rosarins via Iminium Activation

Duong D. Nguyen,[a] Jorge Labella,[*b] Marta Gómez-Gómez,[b] Tomás Torres,[*b,c,d] and Jonathan L. Sessler. [*a]

[a.] *Department of Chemistry, The University of Texas at Austin, 105 E 24th Street A5300, Austin, TX, 78712, United States. E-mail: sessler@cm.utexas.edu*
[b.] *Departamento de Química Orgánica, Universidad Autónoma de Madrid, Campus de Cantoblanco, C/ Francisco Tomás y Valiente 7, 28049 Madrid (Spain) E-mail: jorge.labella; tomas.torres@uam.es*
[c.] *Institute for Advanced Research in Chemical Sciences (IAdChem), Universidad Autónoma de Madrid, 28049 Madrid, Spain*
[d.] *IMDEA-Nanociencia, Campus de Cantoblanco, 28049 Madrid, Spain*

Table of Contents

1. Instrumentation and Materials

Reaction progress was monitored by thin layer chromatography (TLC), employing aluminum sheets coated with silica gel type 60 F254 (0.2 mm thick, Merck) and either a 254 or 365 nm UV lamp. Purification and separation of the synthesized products was performed by normal-phase column chromatography, using silica gel (230–400 mesh, 0.040–0.063 mm, Merck) and size exclusion chromatography, using Bio-Beads^{TM} S-X1 (styrene divinylbenzene beads, 40-80 μm bead size, Bio-Rad). Eluents, along with the relative ratios in the case of solvent mixtures, are indicated for each particular case. Nuclear magnetic resonance spectra (^{1}H, ^{13}C, ^{19}F NMR) were recorded on Agilent MR400, Bruker AV-400, Bruker DRX-500 or Varian MR600 spectrometers at the Department of Chemistry of The University of Texas at Austin (UT Austin). The deuterated solvent employed in each case is indicated in brackets, and its residual peak was used to calibrate the spectra using literature reference δ ppm values.[1] The peaks marked with asterisks indicates residual solvent signals. The NMR spectroscopic solvents were purchased from Cambridge Isotope Laboratories or Fischer Scientific. All spectra were recorded at room temperature. High resolution ESI mass spectrometry was carried out using an Ion Spec Fourier Transform mass spectrometer (9.4 T). Electrospray ionization (ESI) mass spectra were recorded on an Agilent Technologies 6530 Accurate-Mass Q-TOF instrument housed in the Department of Chemistry, UT Austin. Ultraviolet-visible (UV-Vis) spectra were recorded using spectroscopic grade solvents using a Varian Cary 5000 spectrophotometer housed in the in the Department of Chemistry, UT Austin. The logarithm of the molar extinction coefficient (ε) is indicated in brackets for each maximum. Electrochemical characterizations were performed with a three-electrode setup on AutoLab PGStat 30 instrument from the Departamento de Química Orgánica of Universidad Autónoma de Madrid. The measurements were carried out in dichloromethane using 0.1 M tetrabutylammonium hexafluorophosphate ($TBAPF_6$) as electrolyte and compound concentration of approx. 10^{-4} M. A platinum rod was used as working electrode, platinum wire served as counter electrode and Ag/AgCl as reference electrode. Ferrocene (Fc) was used as the internal standard and all the potentials were noted relative to the Fc/Fc^{+} couple. Scan rate was 100 mV s^{-1}. The data were recorded with the NOVA 2.0 software. Chemicals were purchased from commercial suppliers and used without further purification. Dry solvents were purchased from commercial suppliers as anhydrous grade or thoroughly dried before use employing standard methods. Solid, hygroscopic reagents were dried in a vacuum oven before use. The synthesis and characterization of naphthobipyrrole and 4-azidotetrafluorobenzaldehyde has been previously reported.[2,3]

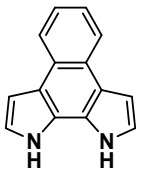

Naphthobipyrrole

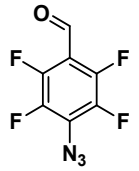

4-azidotetrafluorobenzaldehyde

2. Synthetic Procedures and Characterization Data

Synthesis and characterization of aldehyde precursors

2,6-Difluoro-3,5-dimethoxybenaldehyde

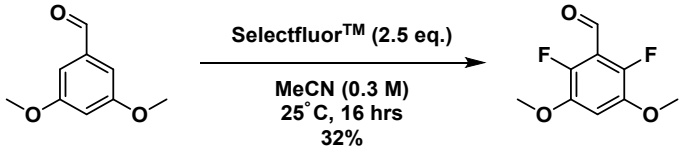

Using an ice bath, a solution of crude 3,5-dimethoxybenzaldehyde in acetonitrile (15 mL) was cooled to 0°C. To this solution, SelectFluor™ (5.2 g, 11 mmol, 2.5 equiv.) was added portion-wise while the temperature was kept below 0°C. The resulting mixture was stirred at 15°C for 16 hours. The reaction mixture was concentrated to remove solvent. The residue was diluted with water (10 mL) and neutralized with saturated aqueous $NaHCO_3$. The product was extracted with ethyl acetate (10 mL x3). The collected organic fraction was then washed with brine (10 mL) and water (10 mL) before being dried over Na_2SO_4 and concentrated *in vacuo*. The resulting crude product was purified via silica gel column chromatography using hexanes: ethyl acetate = 4:1 as the eluent. **Yield** 0.28 g, 32%, light yellow crystalline solid. **^{1}H NMR** (400 MHz, $CDCl_3$) δ 10.35 (s, 1H), 6.88 (t, J = 8.0 Hz, 1H), 3.91 (s, 6H). **^{13}C NMR** (101 MHz, $CDCl_3$) δ 184.72, 147.41, 144.81, 143.75, 106.87, 57.47. **^{19}F NMR** (376 MHz, $CDCl_3$) δ -147.76 (d, J = 7.9 Hz). **HRMS** (ESI positive): *m/z* [M+Na^+] Calculated for $C_9H_8F_2O_3$: 225.0334, found: 225.0338.

4-((4-Bromophenyl)thio)-2,3,5,6-tetrafluorobenzaldehyde

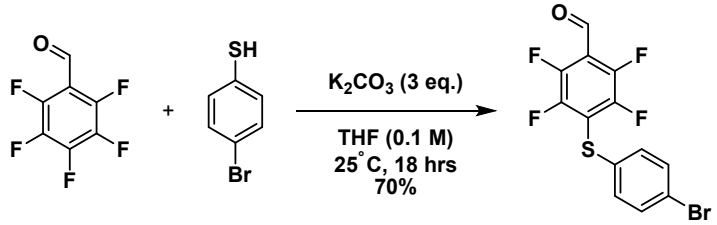

In a 250 mL round bottomed flask, a mixture of pentafluorobenzaldehyde (2.0 g, 10.2 mmol, 1 equiv.) and 4-bromobenzenethiol (1.93 g, 10.2 mmol, 1 equiv.) was dissolved in THF (100 mL). The solution was then deoxygenated for 10 minutes by bubbling with nitrogen gas. To the resulting solution, K_2CO_3 (4.23 g, 30.6 mmol, 3 equiv.) was added in one portion. Then, the resulting mixture was stirred at 25°C for 18 hours. The reaction mixture was concentrated to remove solvent. The residue was diluted with water (30 mL) extracted with ethyl acetate (10 mL x3). The combined organic fractions were then washed with brine (10 mL) and water (10 mL) before being dried over Na_2SO_4 and concentrated *in vacuo*. The resulting crude product was purified via silica gel column chromatography using hexanes: ethyl acetate = 4:1 as the eluent. **Yield** 2.6 g, 70%, yellow powder. **^{1}H NMR** (400 MHz, $CDCl_3$) δ 10.29 (s, 1H), 7.49 – 7.44 (m, 2H), 7.32 (d, J = 8.4 Hz, 2H). **^{13}C NMR** (101 MHz, $CDCl_3$) δ 182.52, 134.01, 133.23, 133.10, 133.07, 131.40, 130.51, 123.90, 115.32, 77.80, 77.48, 77.16, 0.46. **^{19}F NMR** (376 MHz, $CDCl_3$) δ -132.18 – -132.34 (m), -144.34 – -144.51 (m). **HRMS** (ESI positive): *m/z* [M+Na^+] Calculated for $C_{13}H_5BrF_4OS$: 364.9253, found: 364.9253.

Synthesis and characterization of naphthorosarin macrocycles

General procedures for the synthesis of naphthorosarin macrocycles

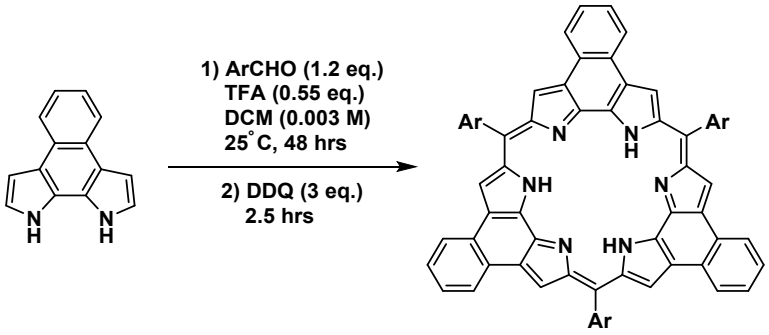

General procedure A (without iminium catalyst):[4] A 1 L round-bottomed flask was charged with naphthobipyrrole (100 mg, 0.484 mmol, 1 equiv.) and aldehyde (1.2 equiv.). Dry dichloromethane (300 mL, 0.0015 M) was then added to dissolve the solids. The reaction mixture was bubbled with nitrogen for 15 minutes and the flask fully covered with aluminum foil. Trifluoroacetic acid (20 μL, 0.26 mmol, 0.55 equiv.) was then slowly added via syringe. The reaction mixture was kept stirring at room temperature for 72 hours under a nitrogen atmosphere. After this time, DDQ (352 mg, 1.55 mmol, 3.2 equiv.) was added, and the reaction mixture was stirred for a further 2.5 hours open to air and light. Once the reaction was deemed complete based on a TLC analysis, excess triethylamine (0.5 mL) was added to the reaction flask and the whole solution was passed through a plug of neutral alumina. Excess dichloromethane (about 200 mL) was used to elute fully the dark purple fraction. The resulting solution was then evaporated to dryness. The crude product obtained in this way was purified via silica gel column chromatography (doped with 1% triethylamine) to obtain the desired solid. Detailed column conditions are given below for each particular rosarin compound. Finally, recrystallization of the solid obtained after removing the volatiles following chromatography from dichloromethane/methanol yielded naphthorosarin as a dark brown solid.

General procedure B (with iminium catalyst): A 1 L round-bottomed flask was charged with naphthobipyrrole (100 mg, 0.484 mmol, 1 equiv.) and aldehyde (1.2 equiv.). Then dry dichloromethane (300 mL, 0.0015 M) and pyrrolidine (20 μL, 0.242 mmol, 0.5 equiv.) was subsequently added. The reaction mixture was bubbled with nitrogen for 15 minutes and the flask fully covered with aluminum foil. Trifluoroacetic acid (0.22 mL, 2.91 mmol, 6 equiv.) was then slowly added via syringe. The reaction mixture was kept stirring at room temperature for 72 hours under a nitrogen atmosphere. After this time, DDQ (352 mg, 1.55 mmol, 3.2 equiv.) was added, and the reaction mixture was stirred for a further 2.5 hours open to air and light. Once the reaction was deemed complete as judged by TLC analysis, excess triethylamine (0.5 mL) was added to the reaction flask and the whole solution was passed through a plug of neutral alumina. Excess dichloromethane (about 200 mL) was used to elute fully the dark purple fraction. The resulting solution was then evaporated to dryness. The crude product was purified via silica gel column chromatography (doped with 1% triethylamine) to give the desired solid. Detailed column conditions are given below for each particular rosarin compound. Finally, recrystallization of the solid from dichloromethane/methanol as per Procedure A yielded naphthorosarin as a dark brown solid.

NRos-1

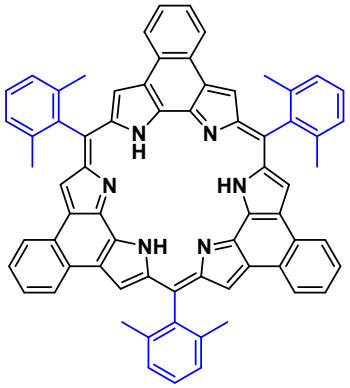

A 1 L round bottomed flask charged with naphthobipyrrole (100 mg, 0.484 mmol, 1 equiv.) and 2,6-dimethylbenaldehyde (78.1 mg, 0.58 mmol, 1.2 equiv.). The general procedures were then followed to obtain a crude product. This crude product was purified via silica gel column chromatography (doped with 1% triethylamine) using hexanes: dichloromethane, gradient of 1:1 to 1:2. Finally, recrystallization of the solid from dichloromethane/methanol yielded **NRos-1** as a dark brown solid. **Yield** 12.5 mg, 8% (procedure B) **^{1}H NMR** (600 MHz, THF-d_8) δ 7.13 – 7.11 (m, 6H), 7.08 (d, J = 6.9 Hz, 3H), 7.00 (d, J = 7.5 Hz, 6H), 6.95 (dq, J = 6.0, 2.7 Hz, 6H), 5.20 (s, 6H), 2.42 (s, 18H). **^{13}C NMR** (151 MHz, THF-d_8) δ 148.78, 144.21, 135.81, 134.77, 130.72, 127.83, 127.32, 125.57, 124.24, 123.48, 123.34, 119.05, 29.63. **HRMS** (ESI positive): *m/z* [M+H$^+$] Calculated for $C_{69}H_{48}N_6$: 961.4013, found: 961.4011. **UV-Vis** (CH_2Cl_2): λ_{max} (nm) (log ε(dm^3 cm^{-1} mol^{-1})): 485 (4.6), 571 (4.3).

NRos-2

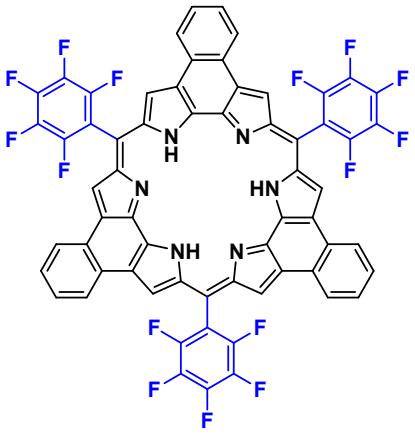

A 1 L round bottomed flask charged with naphthobipyrrole (100 mg, 0.484 mmol, 1 equiv.) and 2,6-dimethylbenaldehyde (114 mg, 0.58 mmol, 1.2 equiv.). The general procedures were then followed to obtain a crude product. This crude product was purified via silica gel column chromatography (doped with 1% triethylamine) using hexanes: dichloromethane, gradient of 1:1 to 1:2. Finally, recrystallization of the solid from dichloromethane/methanol yielded **NRos-2** as a dark brown solid. **Yield** 28 mg, 15% (procedure A); 37 mg, 20% (procedure B). **^{1}H NMR** (400 MHz, THF-d_8) δ 7.00 (d, J = 19.1 Hz, 12H), 5.13 (s, 6H). **^{19}F NMR** (376 MHz, THF-d_8) δ -140.02, -154.77, -160.95. The yield (procedure A), ^{1}H NMR and ^{19}F NMR

spectra roved concordant with previously published data.[4] **UV-Vis** (CH_2Cl_2) : λ_{max} (nm) (log ε($dm^3\ cm^{-1}\ mol^{-1}$)): 463 (5.1), 588 (4.7).

NRos-3

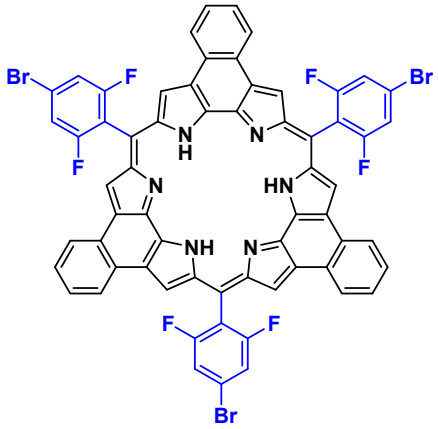

A 1 L round bottomed flask charged with naphthobipyrrole (100 mg, 0.484 mmol, 1 equiv.) and 2,6-dimethylbenaldehyde (129 mg, 0.58 mmol, 1.2 equiv.). The general procedures were then followed to obtain a crude product. This crude product was purified via silica gel column chromatography (doped with 1% triethylamine) using hexanes: dichloromethane, gradient of 1:1 to 1:2. Finally, recrystallization of the solid from dichloromethane/methanol yielded **NRos-3** as a dark brown solid. **Yield** 21 mg, 18% (procedure A); 37.8 mg, 15% (procedure B). **^{1}H NMR** (600 MHz, THF-d_8) δ 7.27 (d, J = 6.8 Hz, 6H), 7.11 (dt, J = 7.1, 3.6 Hz, 6H), 6.96 (dd, J = 6.0, 3.4 Hz, 6H), 5.15 (s, 6H). **^{13}C NMR** (151 MHz, THF-d_8) δ 132.47, 131.97, 126.95, 124.83, 124.51, 123.78, 120.46, 117.07, 117.04, 116.88, 112.74, 112.60. **^{19}F NMR** (376 MHz, THF-d_8) δ -109.50. **HRMS** (ESI positive): *m/z* [M+H$^+$] Calculated for $C_{63}H_{27}Br_3F_6N_6$: 1218.9824, found: 1218.9791. **UV-Vis** (CH_2Cl_2): λ_{max} (nm) (log ε($dm^3\ cm^{-1}\ mol^{-1}$)): 472 (5.1), 570 (4.8).

NRos-4

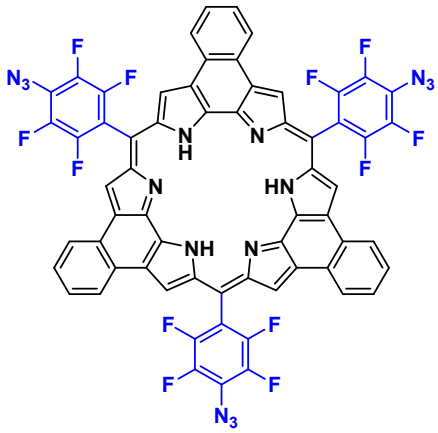

A 1 L round bottomed flask charged with naphthobipyrrole (100 mg, 0.484 mmol, 1 equiv.) and 2,6-dimethylbenaldehyde (107 mg, 0.58 mmol, 1.2 equiv.). The general procedures were then followed to obtain a crude product. This crude product was purified via silica gel column chromatography (doped with 1% triethylamine) using hexanes: dichloromethane, gradient of 1:1 to 1:2. Finally, recrystallization of the solid from dichloromethane/methanol yielded **NRos-4** as a dark brown solid. **Yield** 23 mg, 12% (procedure A); 31 mg, 16% (procedure B). **^{1}H NMR**

(400 MHz, THF-d_8) δ 7.04 (dt, J = 6.9, 3.6 Hz, 6H), 6.99 (dt, J = 5.9, 3.5 Hz, 6H), 5.14 (s, 6H). **^{13}C NMR** (151 MHz, THF-d_8) δ 146.58, 144.95, 143.50, 141.95, 132.81, 131.33, 127.81, 125.35, 125.16, 122.44, 121.18, 111.31. **^{19}F NMR** (376 MHz, THF-d_8) δ -142.30 – -142.58 (m), -152.03 – -152.28 (m). **HRMS** (ESI positive): *m/z* [M+H$^+$] Calculated for $C_{63}H_{21}F_{12}N_{15}$: 1216.1986, found: 1216.1973. **UV-Vis** (CH_2Cl_2): λ_{max} (nm) (log ε(dm^3 cm^{-1} mol^{-1})): 473 (4.8), 585 (4.5).

NRos-5

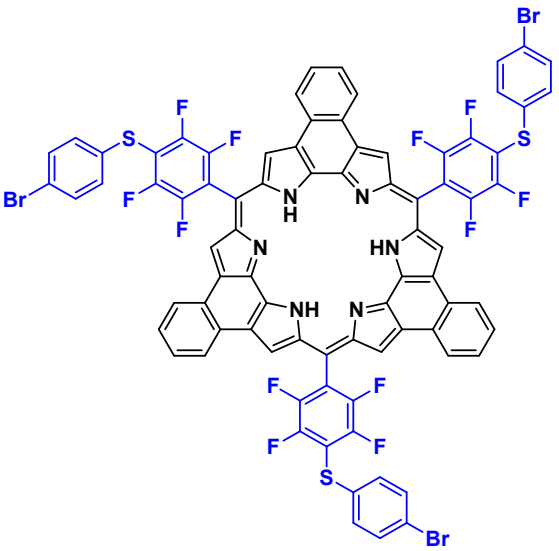

A 1 L round bottomed flask charged with naphthobipyrrole (100 mg, 0.484 mmol, 1 equiv.) and 2,6-dimethylbenaldehyde (192 mg, 0.58 mmol, 1.2 equiv.). The general procedures were then followed to obtain a crude product. This crude product was purified via silica gel column chromatography (doped with 1% triethylamine) using hexanes: dichloromethane, gradient of 1:1 to 1:2. Finally, recrystallization of the solid from dichloromethane/methanol yielded **NRos-5** as a dark brown solid. **Yield** 35 mg, 13% (procedure A); 50 mg, 19% (procedure B). **^{1}H NMR** (400 MHz, THF-d_8) δ 7.48 (d, J = 8.2 Hz, 6H), 7.31 (d, J = 8.2 Hz, 6H), 7.05 (dt, J = 7.5, 3.7 Hz, 6H), 6.98 (dt, J = 6.0, 3.7 Hz, 6H), 5.13 (s, 6H). **^{13}C NMR** (151 MHz, THF-d_8) δ 149.04, 147.39, 145.85, 144.29, 133.61, 133.28, 132.92, 132.22, 130.78, 127.13, 124.63, 124.56, 123.06, 120.51, 116.52, 114.87. **^{19}F NMR** (376 MHz, THF-d_8) δ -130.97 (dd, J = 24.7, 12.0 Hz), -138.86 (dd, J = 24.7, 11.9 Hz). **HRMS** (ESI positive): *m/z* [M+H$^+$] Calculated for $C_{81}H_{33}Br_3F_{12}N_6S_3$: 1650.9360, found: 1650.9456. **UV-Vis** (CH_2Cl_2): λ_{max} (nm) (log ε(dm^3 cm^{-1} mol^{-1})): 470 (4.9), 572 (4.7).

NRos-6

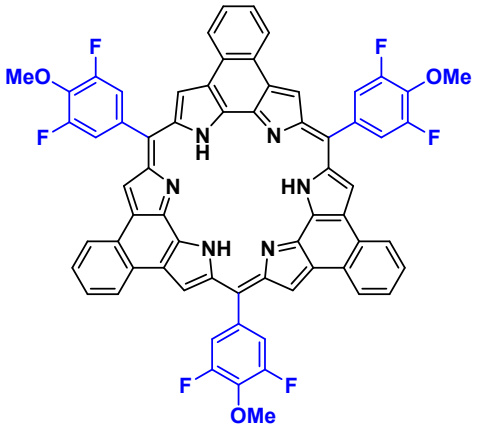

A 1 L round bottomed flask charged with naphthobipyrrole (100 mg, 0.484 mmol, 1 equiv.) and 2,6-dimethylbenaldehyde (100 mg, 0.58 mmol, 1.2 equiv.). The general procedures were then followed to obtain a crude product. This crude product was purified via silica gel column chromatography (doped with 1% triethylamine) using hexanes: dichloromethane, gradient 1:2 to 1:3. Finally, recrystallization of the solid from dichloromethane/methanol yielded **NRos-6** as a dark brown solid. **Yield** 8.6 mg, 7% (procedure A); 24.3 mg, 15% (procedure B). **^{1}H NMR** (600 MHz, THF-d_8) δ 6.97 (d, J = 7.1 Hz, 6H), 6.94 – 6.87 (m, 6H), 6.64 (d, J = 8.5 Hz, 6H), 5.20 (s, 6H), 3.92 (s, 9H). **^{13}C NMR** (151 MHz, THF-d_8) δ 157.31, 155.66, 151.13, 150.14, 138.07, 132.22, 131.25, 126.84, 125.19, 124.31, 121.92, 113.88, 62.13. **^{19}F NMR** (376 MHz, THF-d_8) δ -127.16. **HRMS** (ESI positive): *m/z* [M+H$^+$] Calculated for $C_{66}H_{36}F_6N_6O_3$: 1075.2826, found: 1075.2795. **UV-Vis** (CH_2Cl_2): λ_{max} (nm) (log ε(dm^3 cm^{-1} mol^{-1})): 481 (5.0), 575 (4.7).

NRos-7

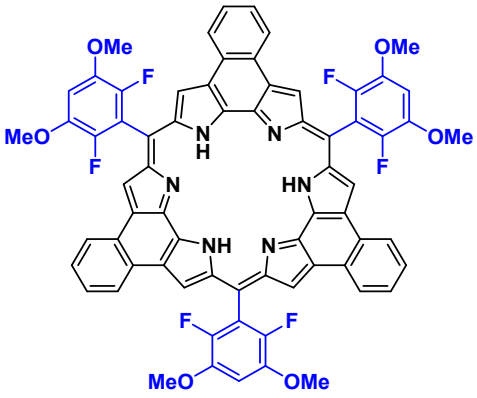

A 1 L round bottomed flask charged with naphthobipyrrole (100 mg, 0.484 mmol, 1 equiv.) and 2,6-dimethylbenaldehyde (118 mg, 0.58 mmol, 1.2 equiv.). The general procedures were then followed to obtain a crude product. This crude product was purified via silica gel column chromatography (doped with 1% triethylamine) using hexanes: dichloromethane, gradient 1:2 to 1:4. Finally, recrystallization of the solid from dichloromethane/methanol yielded **NRos-7** as a dark brown solid. **Yield** 7.5 mg, 4% (procedure A); 22 mg, 12% (procedure B). **^{1}H NMR** (600 MHz, THF-d_8) δ 7.09 (dd, J = 6.0, 3.4 Hz, 6H), 6.95 (dd, J = 6.0, 3.4 Hz, 6H), 6.81 – 6.76 (m, 3H), 5.14 (s, 6H), 3.81 (s, 18H). **^{13}C NMR** (151 MHz, THF-d_8) δ 150.72, 145.01, 144.33, 142.73, 133.81, 131.69, 126.73, 124.96, 124.45, 120.58, 114.47, 101.97, 57.37. **^{19}F NMR** (376 MHz, THF-d_8) δ -143.29 (d, J = 8.1 Hz). **HRMS** (ESI positive): *m/z* [M+H$^+$] Calculated for $C_{69}H_{42}F_6N_6O_3$: 1165.3143, found: 1165.3145. **UV-Vis** (CH_2Cl_2): λ_{max} (nm) (log ε(dm^3 cm^{-1} mol^{-1})): 476 (5.1), 575 (4.8).

NRos-8

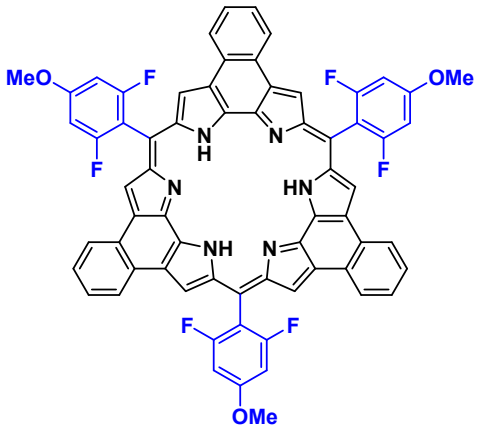

A 1 L round bottomed flask charged with naphthobipyrrole (100 mg, 0.484 mmol, 1 equiv.) and 2,6-dimethylbenaldehyde (100 mg, 0.58 mmol, 1.2 equiv.). The general procedures were then followed to obtain a crude product. This crude product was purified via silica gel column chromatography (doped with 1% triethylamine) using hexanes: dichloromethane, gradient 1:2 to 1:3. Finally, recrystallization of the solid from dichloromethane/methanol yielded **NRos-8** as a dark brown solid. **Yield** 12 mg, 7% (procedure A); 26 mg, 15% (procedure B). **^{1}H NMR** (600 MHz, THF-d_8) δ 7.11 (dd, J = 6.1, 3.3 Hz, 6H), 6.96 (dd, J = 6.0, 3.4 Hz, 6H), 6.56 (d, J = 9.3 Hz, 6H), 5.20 (s, 6H), 3.77 (s, 9H). **^{13}C NMR** (151 MHz, THF-d_8) δ 162.92, 162.59, 161.01, 133.82, 131.62, 126.76, 125.00, 124.39, 120.63, 105.40, 99.27, 99.08, 56.55. **^{19}F NMR** (376 MHz, THF-d_8) δ -112.26. **HRMS** (ESI positive): *m/z* [M+H$^+$] Calculated for $C_{66}H_{36}F_6N_6O_3$: 1075.2826, found: 1075.2824. **UV-Vis** (CH_2Cl_2): λ_{max} (nm) (log ε(dm^3 cm^{-1} mol^{-1})): 481 (5.0), 585 (4.7).

3. NMR Spectra

2,6-Difluoro-3,5-dimethoxybenaldehyde

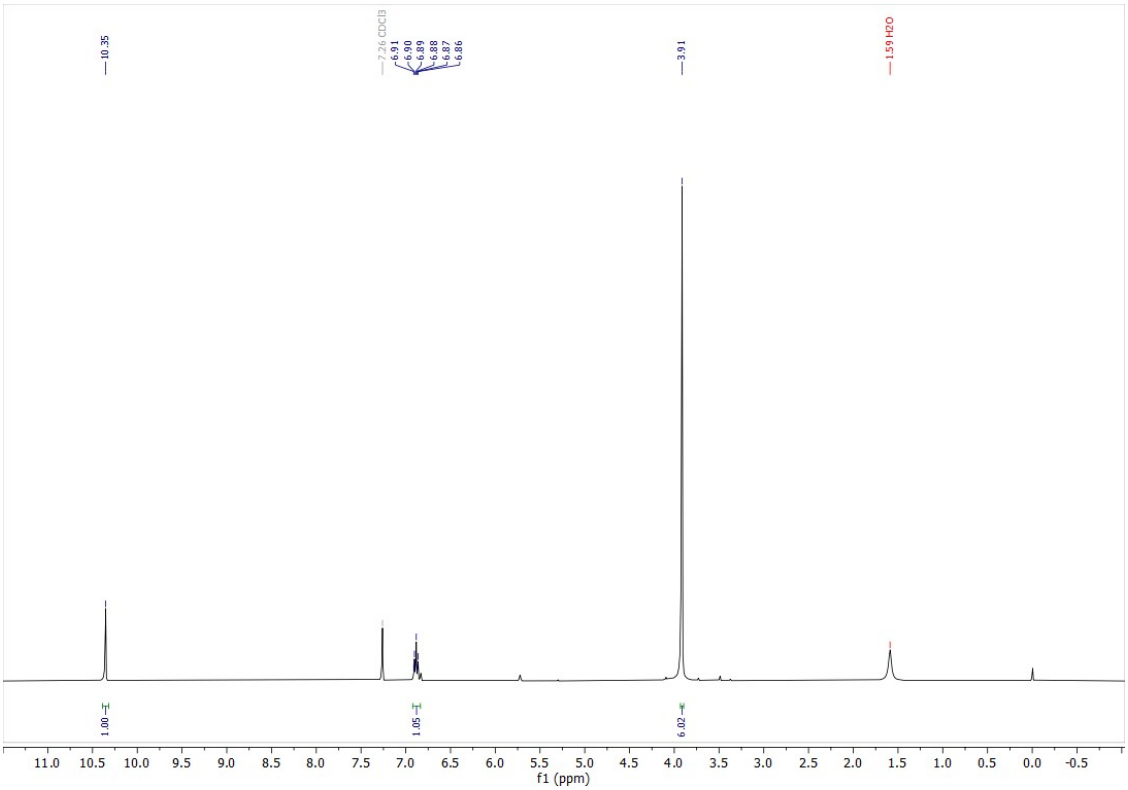

Figure S3.1. ^{1}H NMR spectrum ($CDCl_3$) of **2,6-difluoro-3,5-dimethoxybenaldehyde**

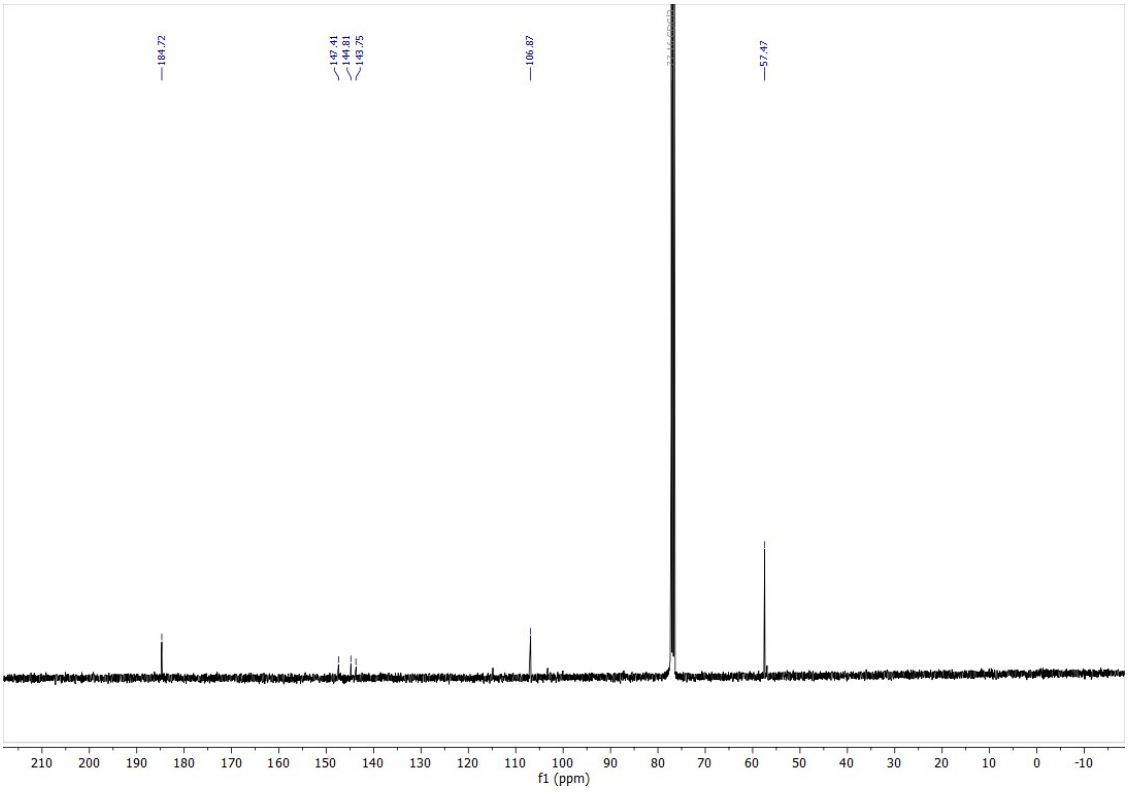

Figure S3.2. ^{13}C NMR spectrum ($CDCl_3$) of **2,6-difluoro-3,5-dimethoxybenaldehyde**

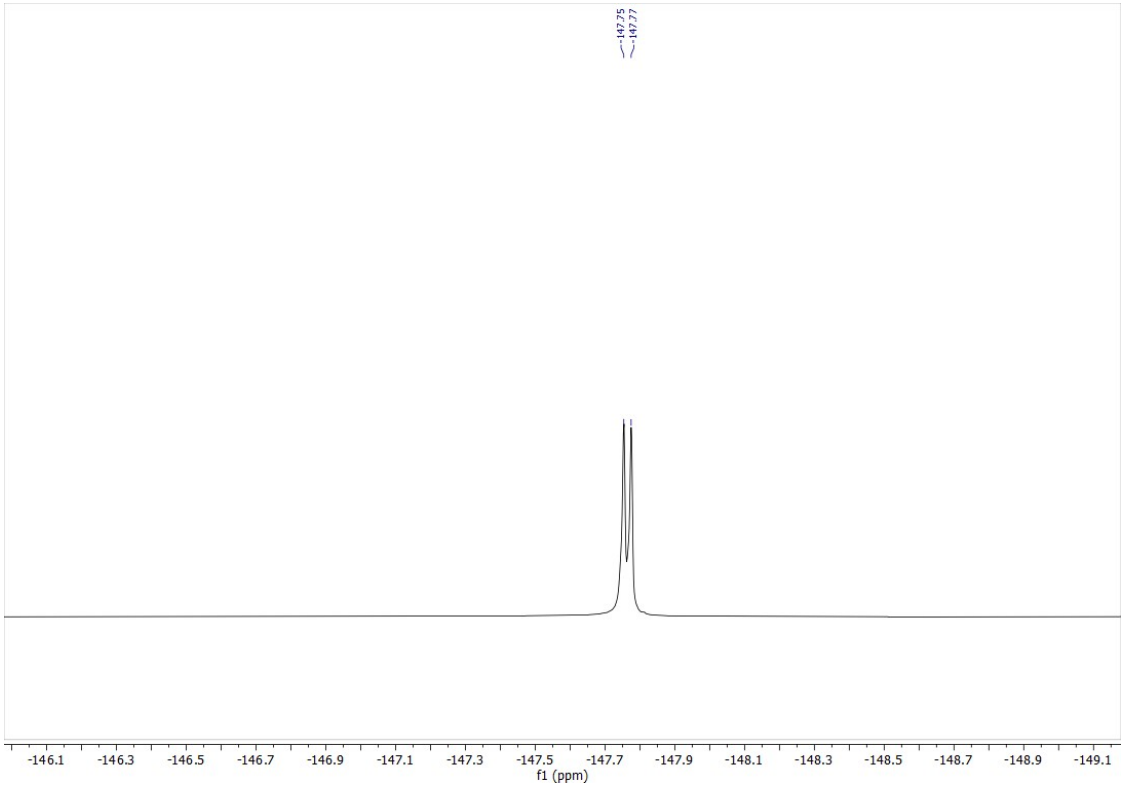

Figure S3.3. ^{19}F NMR spectrum ($CDCl_3$) of **2,6-difluoro-3,5-dimethoxybenaldehyde**

4-((4-Bromophenyl)thio)-2,3,5,6-tetrafluorobenzaldehyde

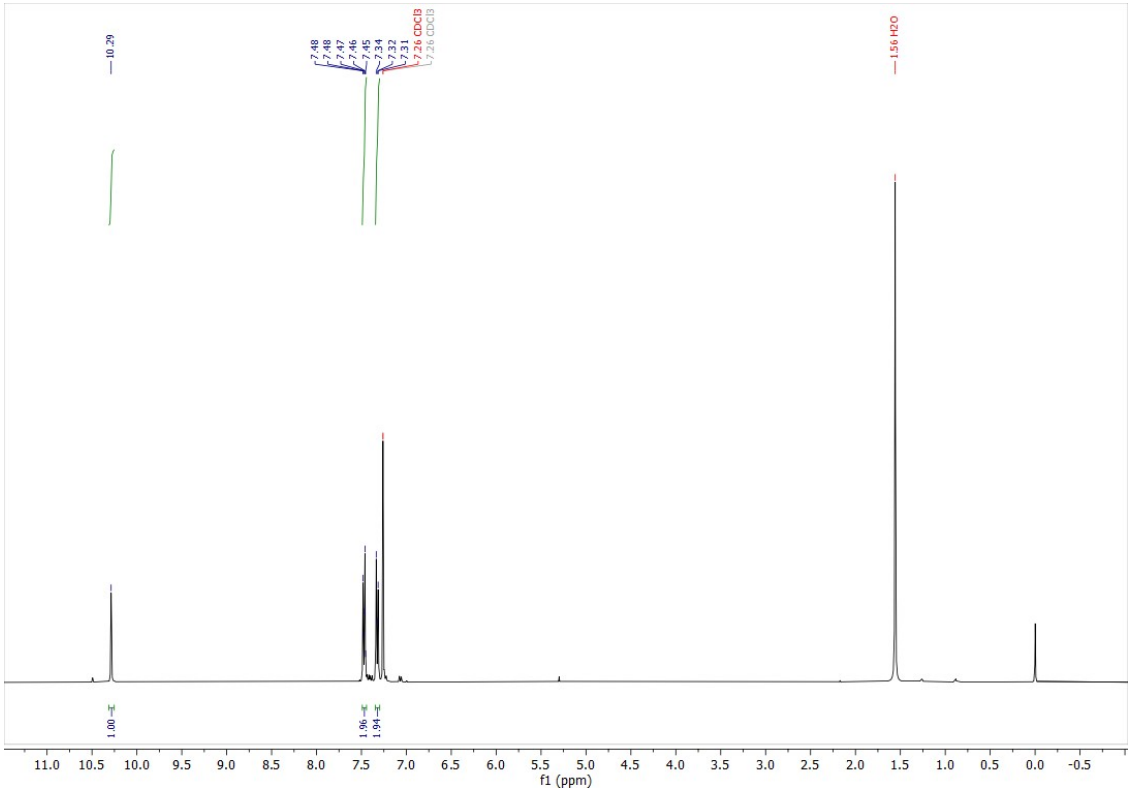

Figure S3.4. ^{1}H NMR spectrum ($CDCl_3$) of **4-((4-bromophenyl)thio)-2,3,5,6-tetrafluorobenzaldehyde**

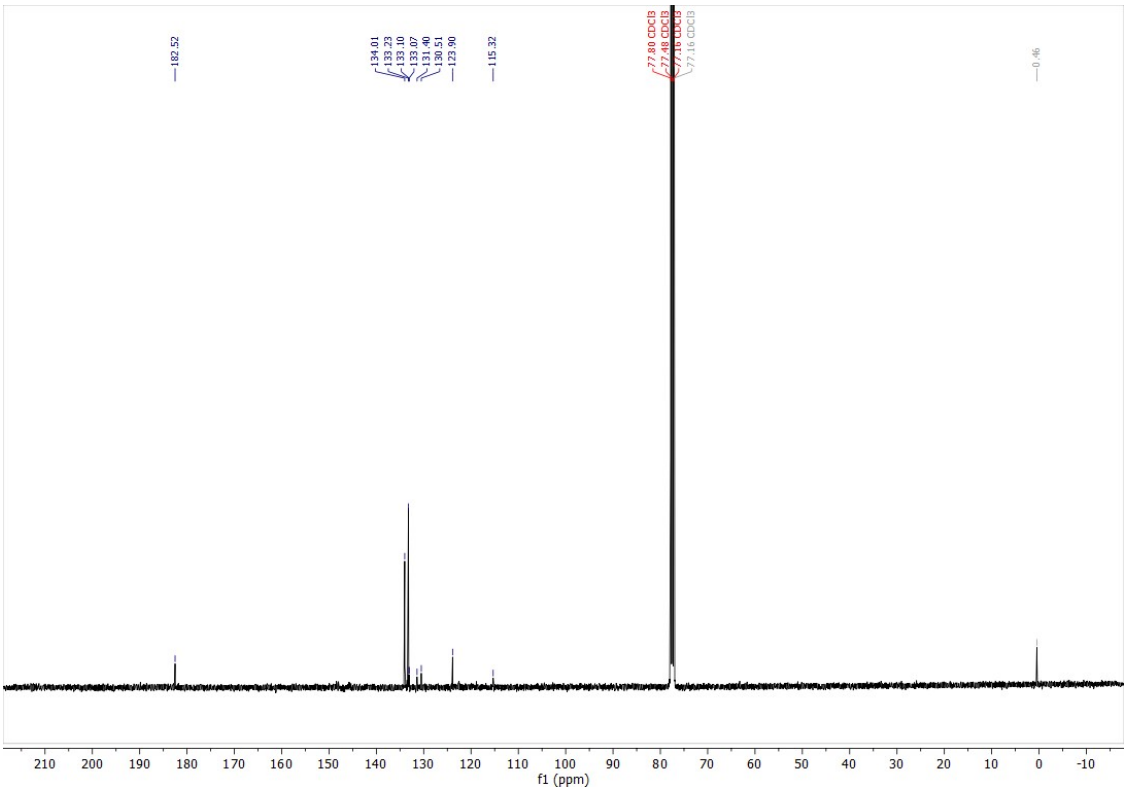

Figure S3.5. ^{13}C NMR spectrum ($CDCl_3$) of **4-((4-bromophenyl)thio)-2,3,5,6-tetrafluorobenzaldehyde**

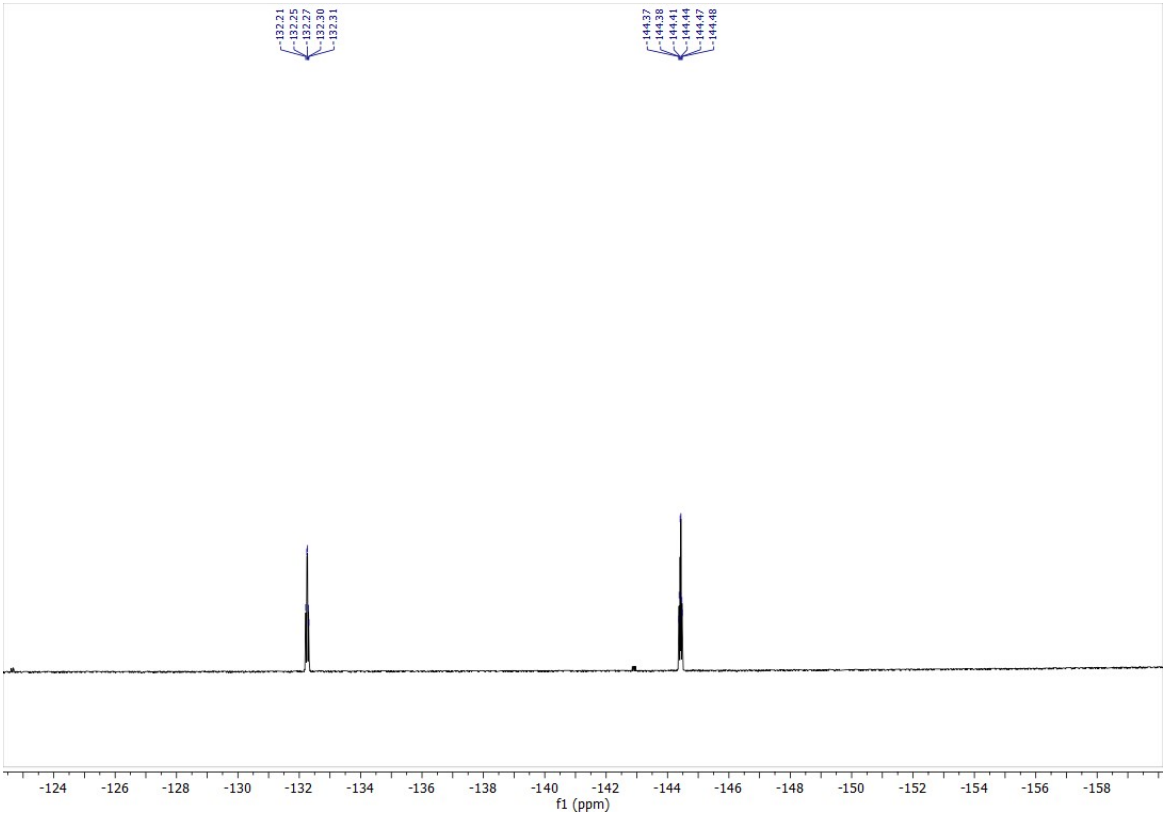

Figure S3.6. ^{19}F NMR spectrum ($CDCl_3$) of **4-((4-bromophenyl)thio)-2,3,5,6-tetrafluorobenzaldehyde**

NRos-1

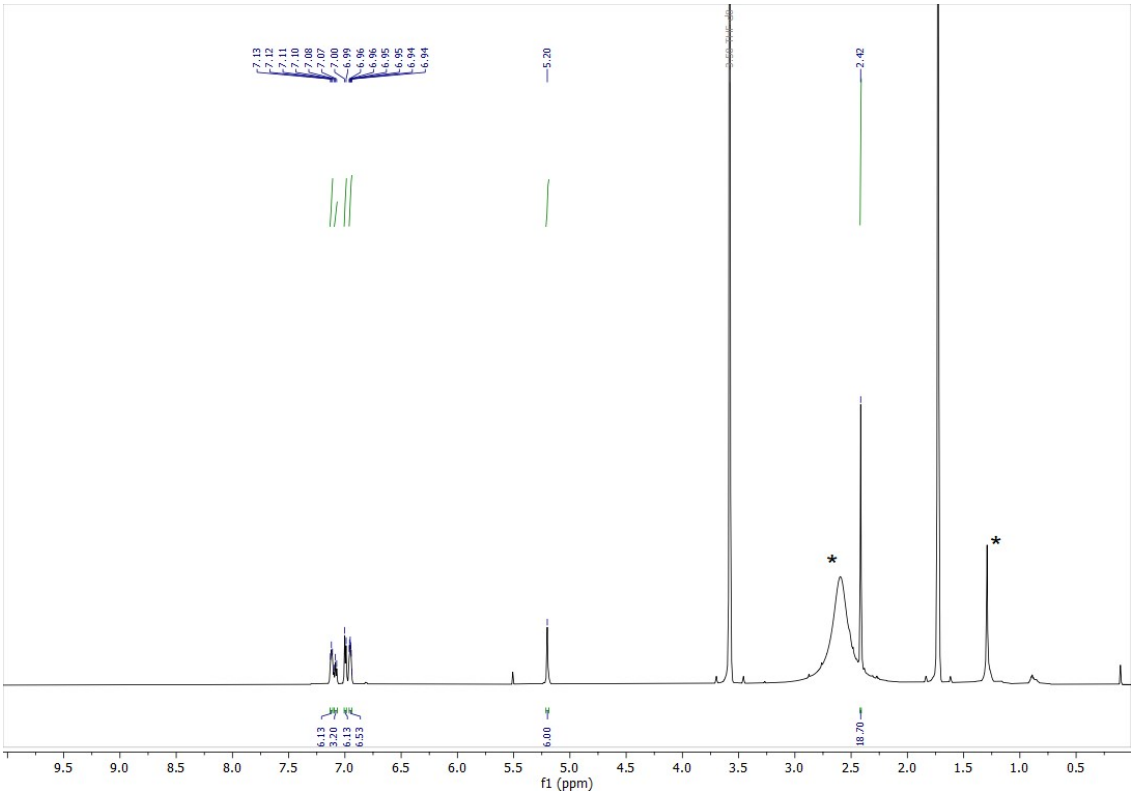

Figure S3.7. ^{1}H NMR spectrum (THF-d_8) of **NRos-1**

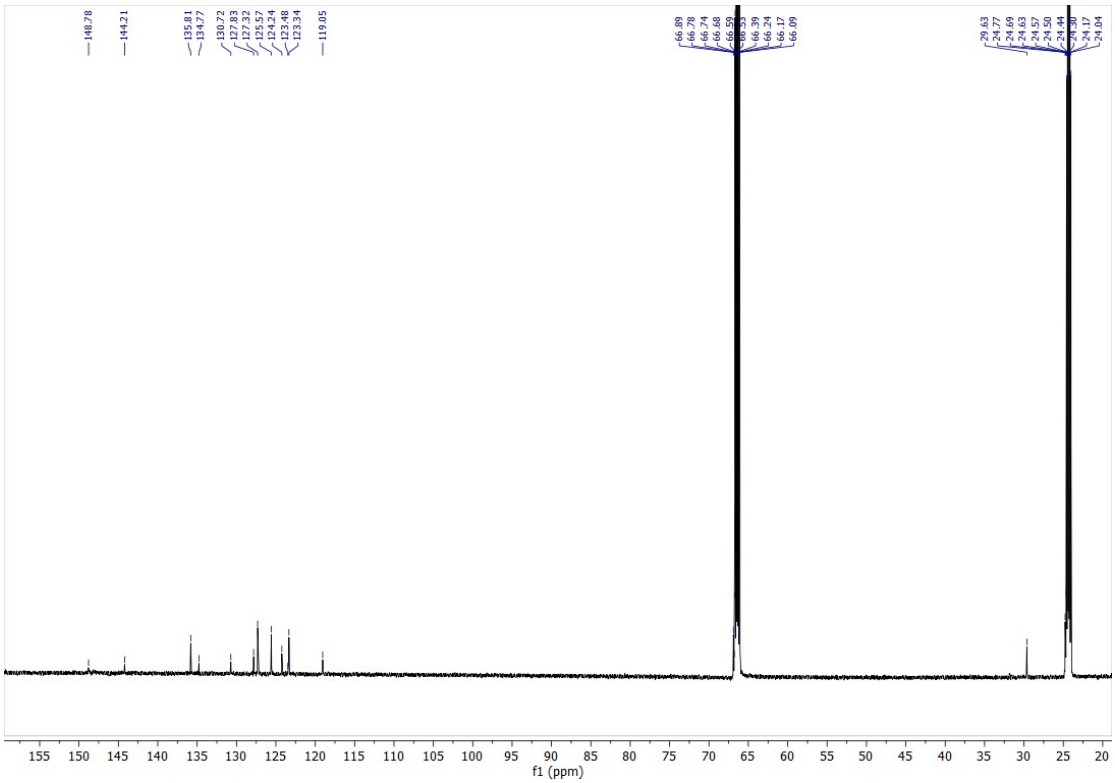

Figure S3.8. ^{13}C NMR (THF-d_8) **NRos-1**

NRos-2

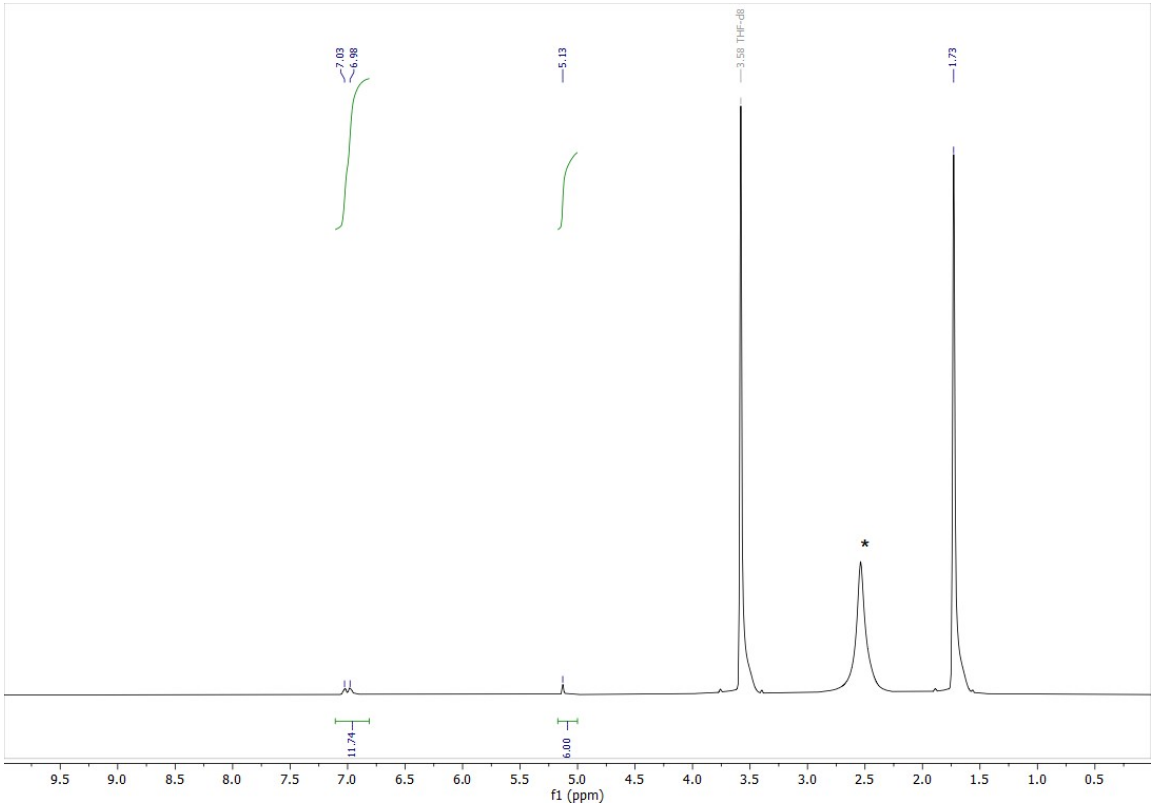

Figure S3.9. ^{1}H NMR spectrum (THF-d_8) of **NRos-2**

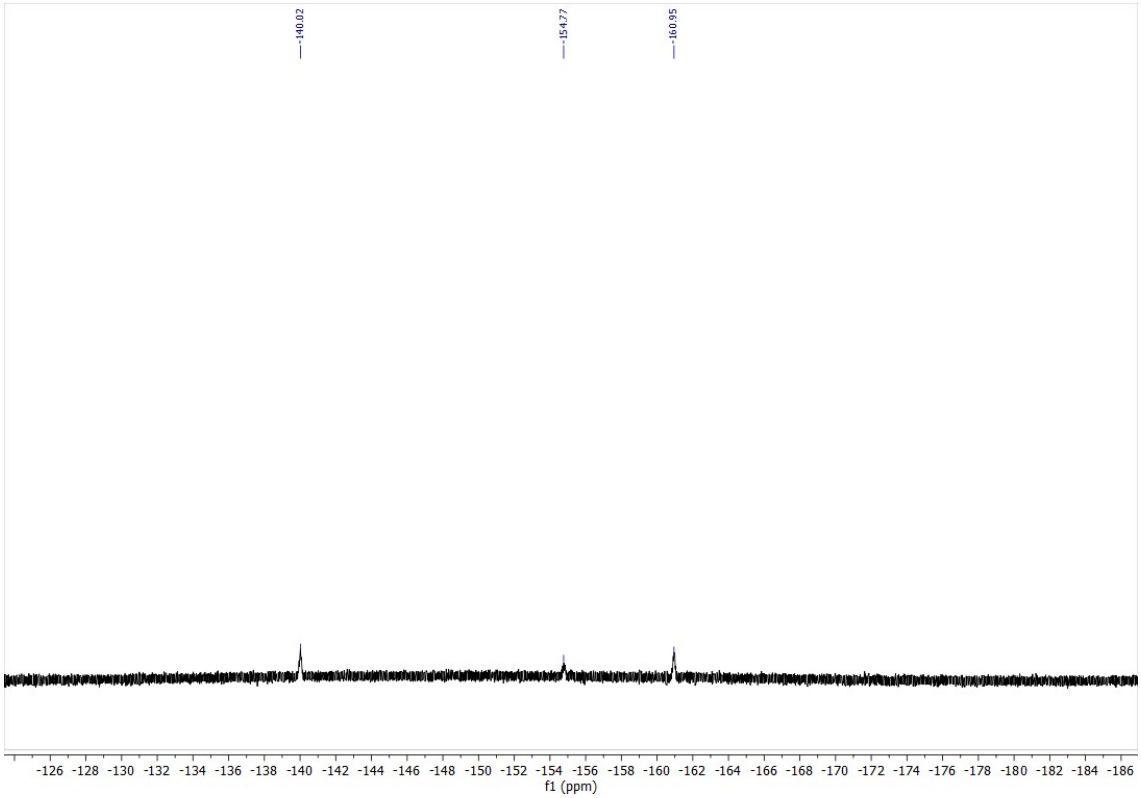

Figure S3.10. ^{19}F NMR spectrum (THF-d_8) of **NRos-2**

NRos-3

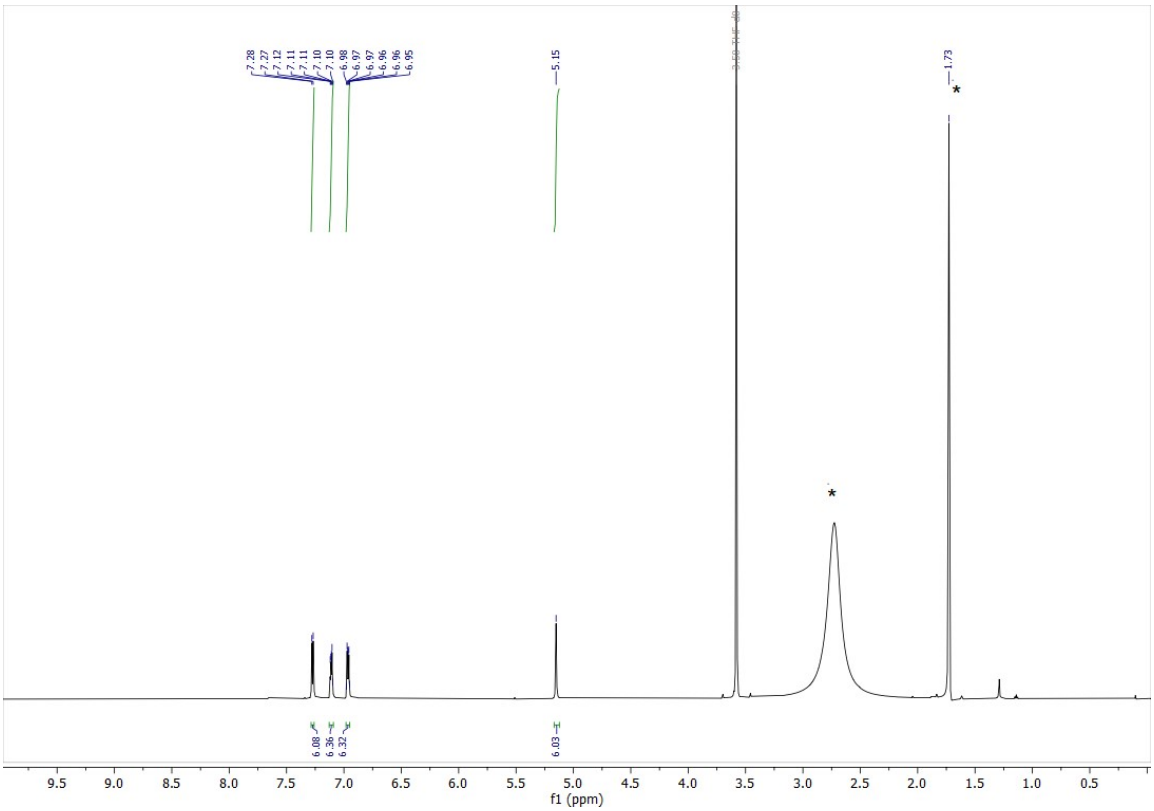

Figure S3.11. ^{1}H NMR spectrum (THF-d_8) of **NRos-3**

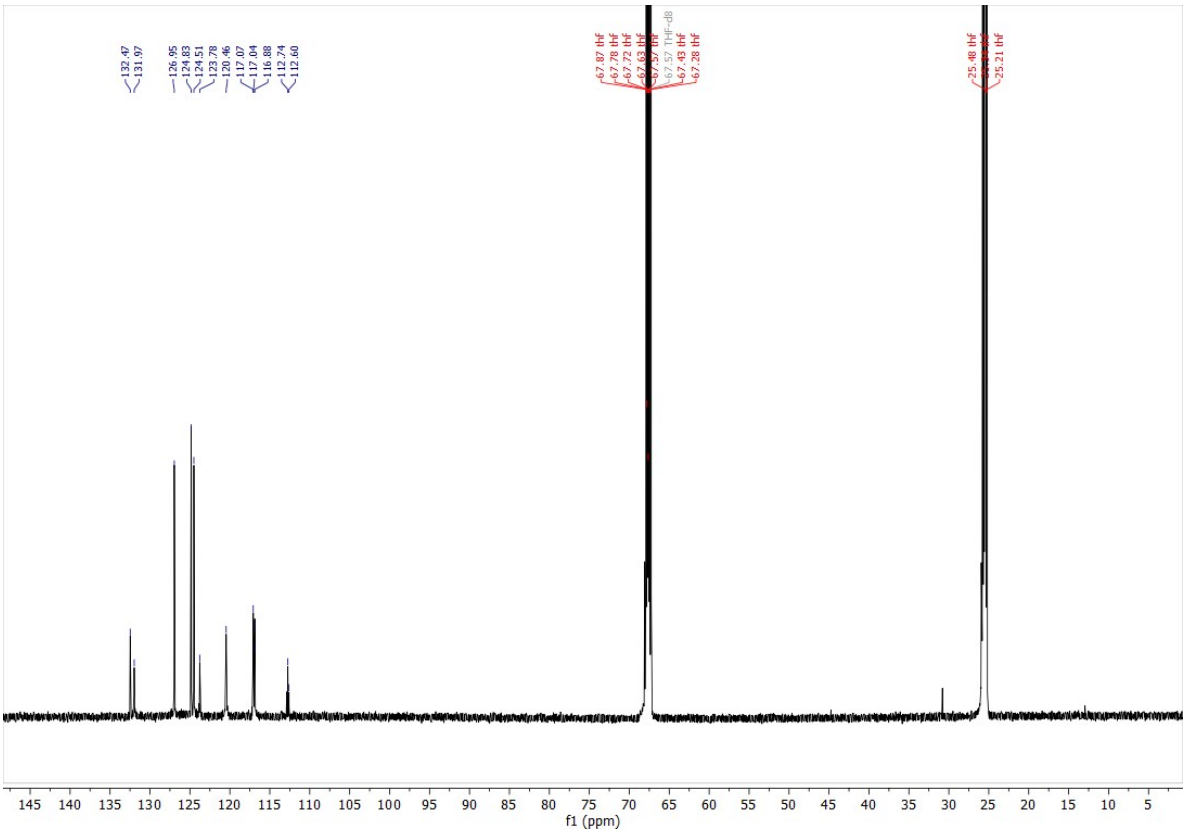

Figure S3.12. ^{13}C NMR spectrum (THF-d_8) of **NRos-3**

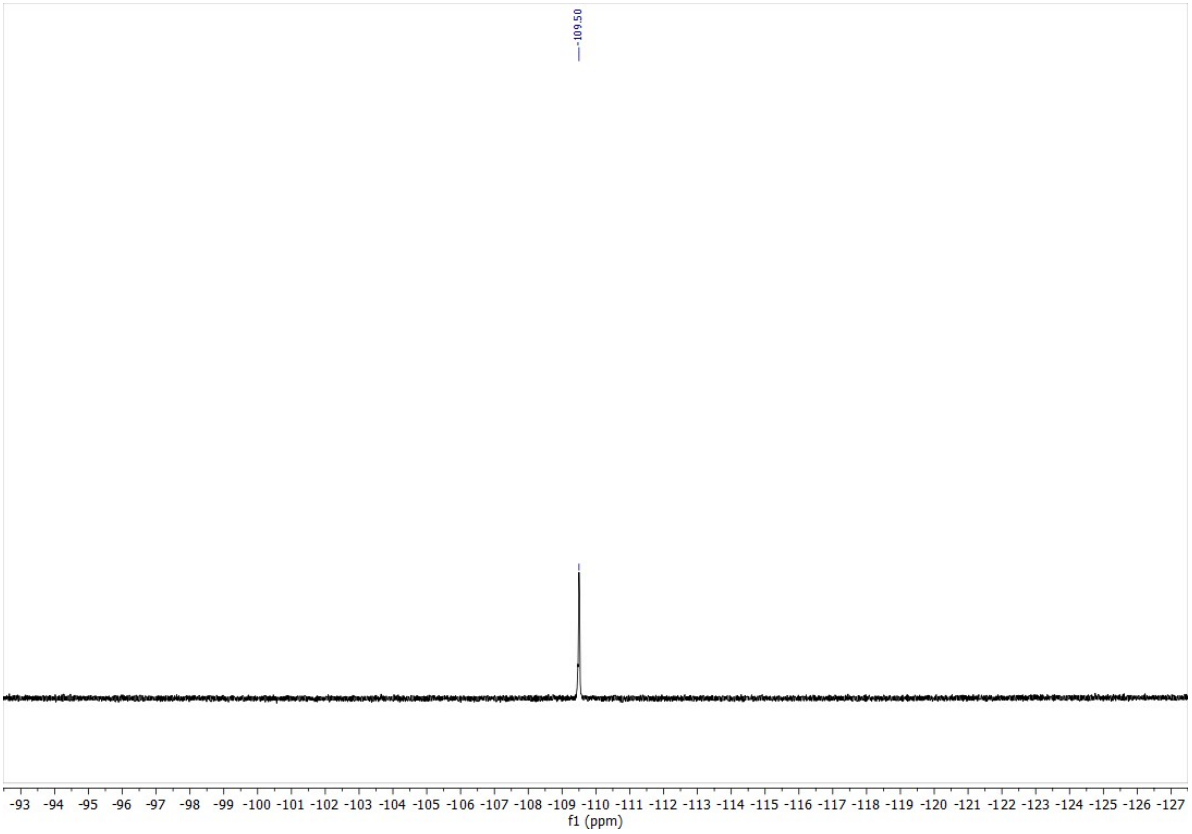

Figure S3.13. ^{19}F NMR spectrum (THF-d_8) of **NRos-3**

NRos-4

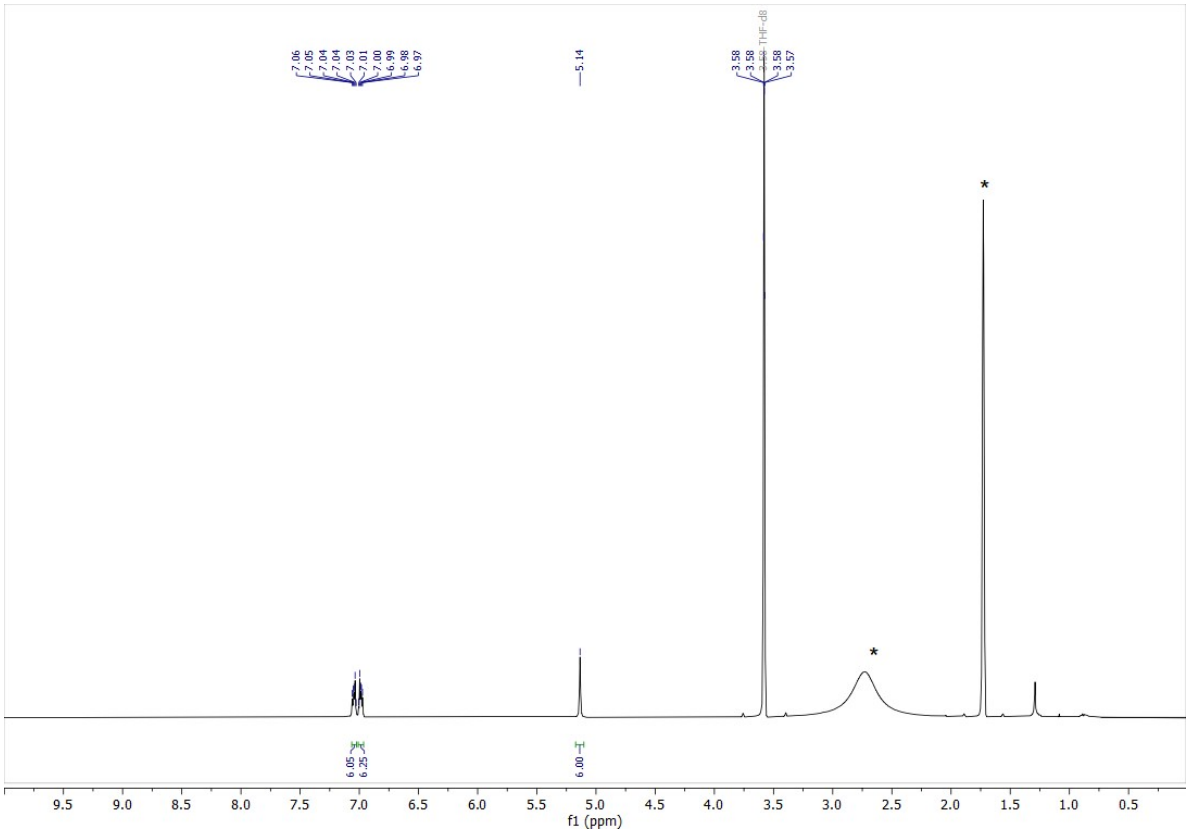

Figure S3.14. ^{1}H NMR spectrum (THF-d_8) of **NRos-4**

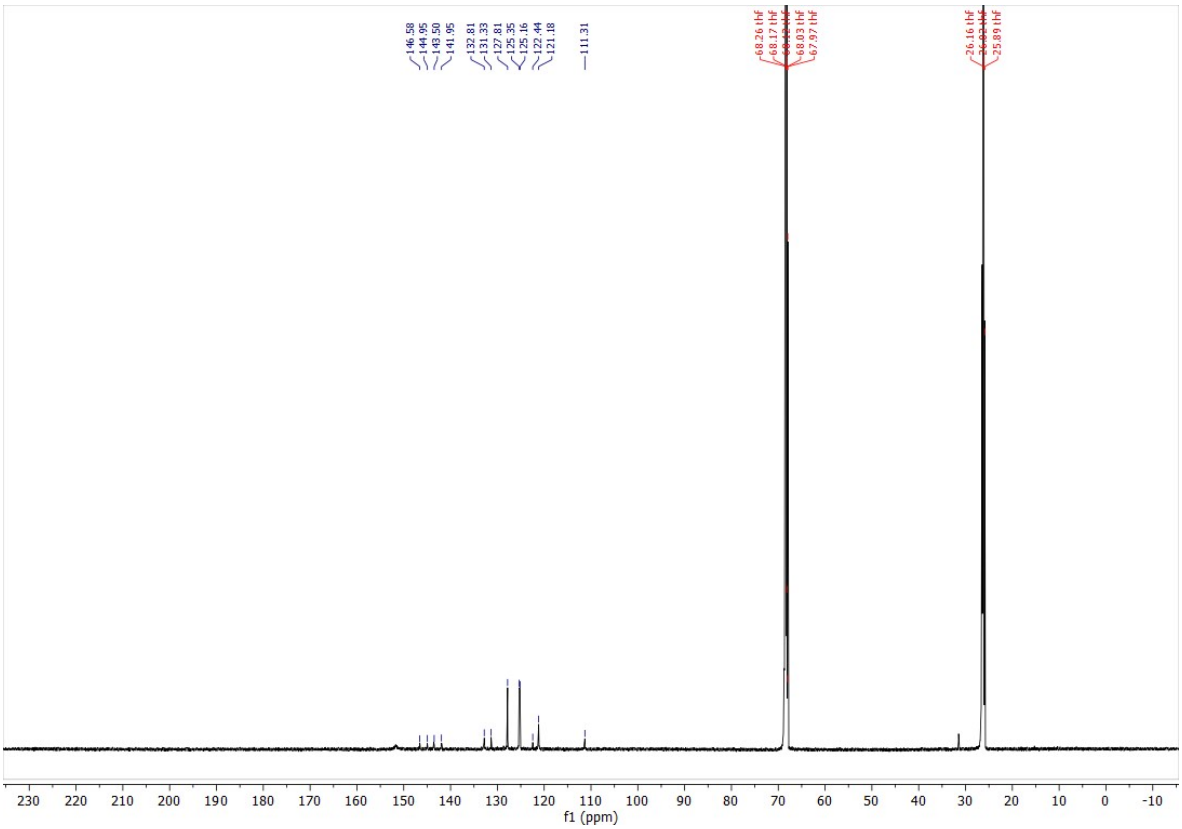

Figure S3.15. ^{13}C NMR spectrum (THF-d_8) of **NRos-4**

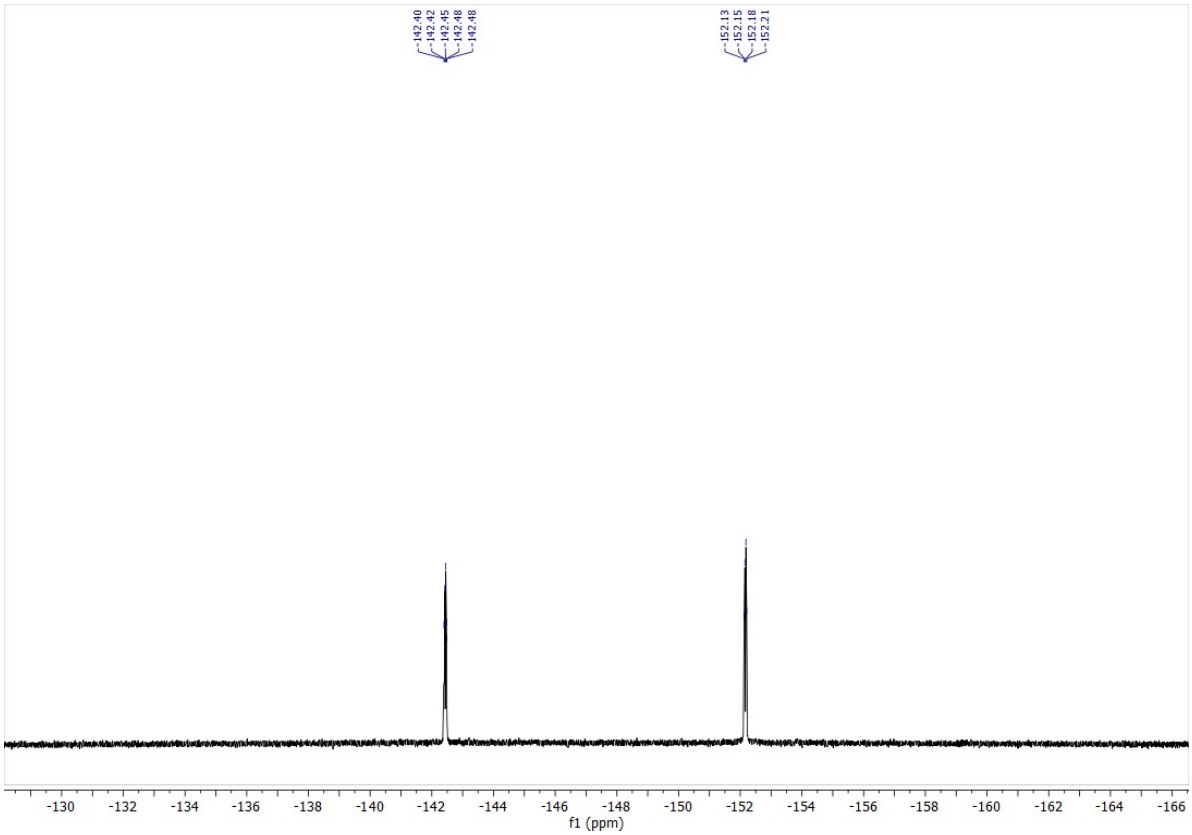

Figure S3.16. ^{19}F NMR spectrum (THF-d_8) of **NRos-4**

NRos-5

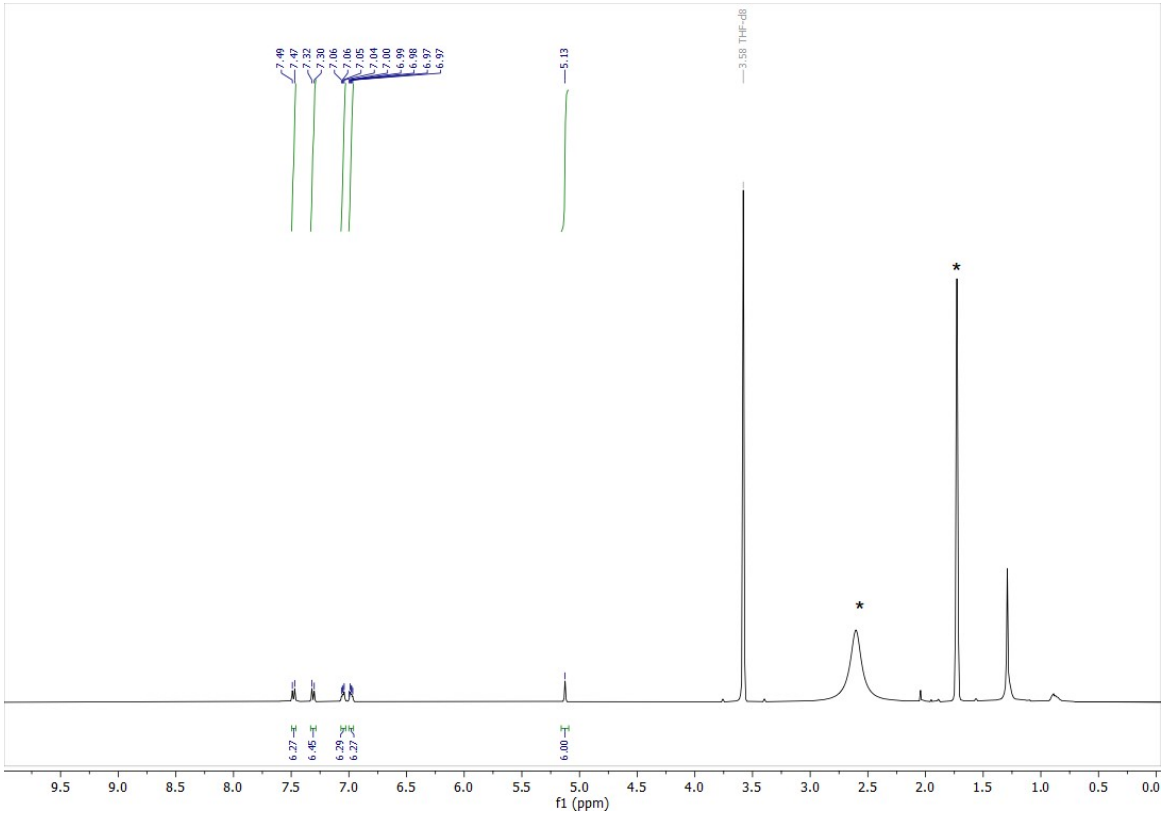

Figure S3.17. ^{1}H NMR spectrum (THF-d_8) of **NRos-5**

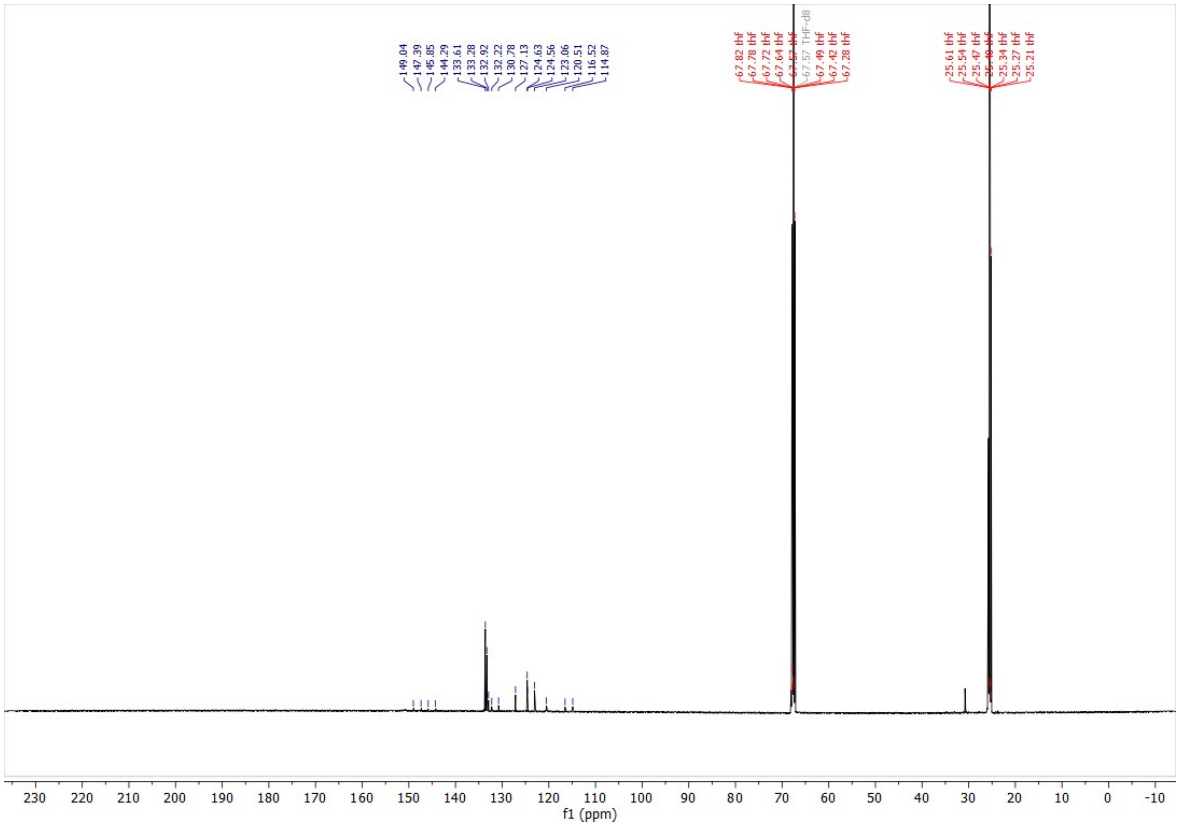

Figure S3.18. ^{13}C NMR spectrum (THF-d_8) of **NRos-5**

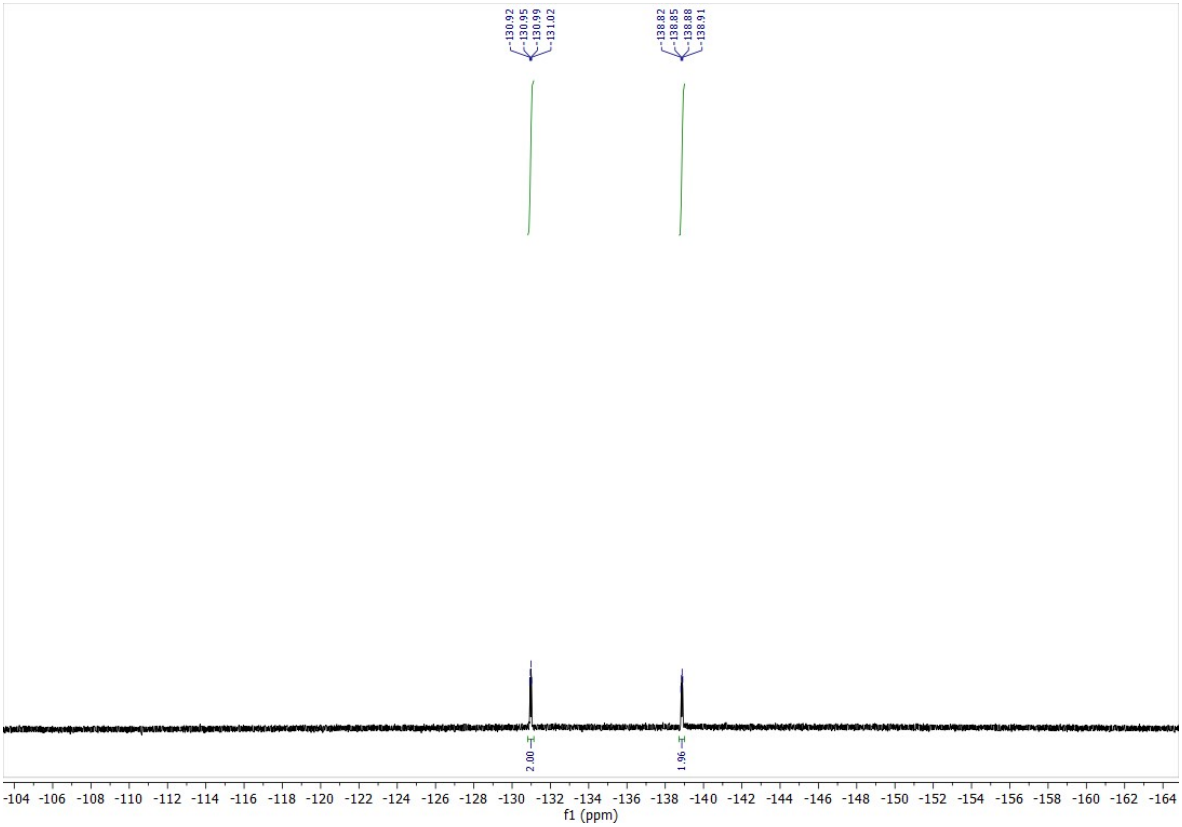

Figure S3.19. ^{19}F NMR spectrum (THF-d_8) of **NRos-5**

NRos-6

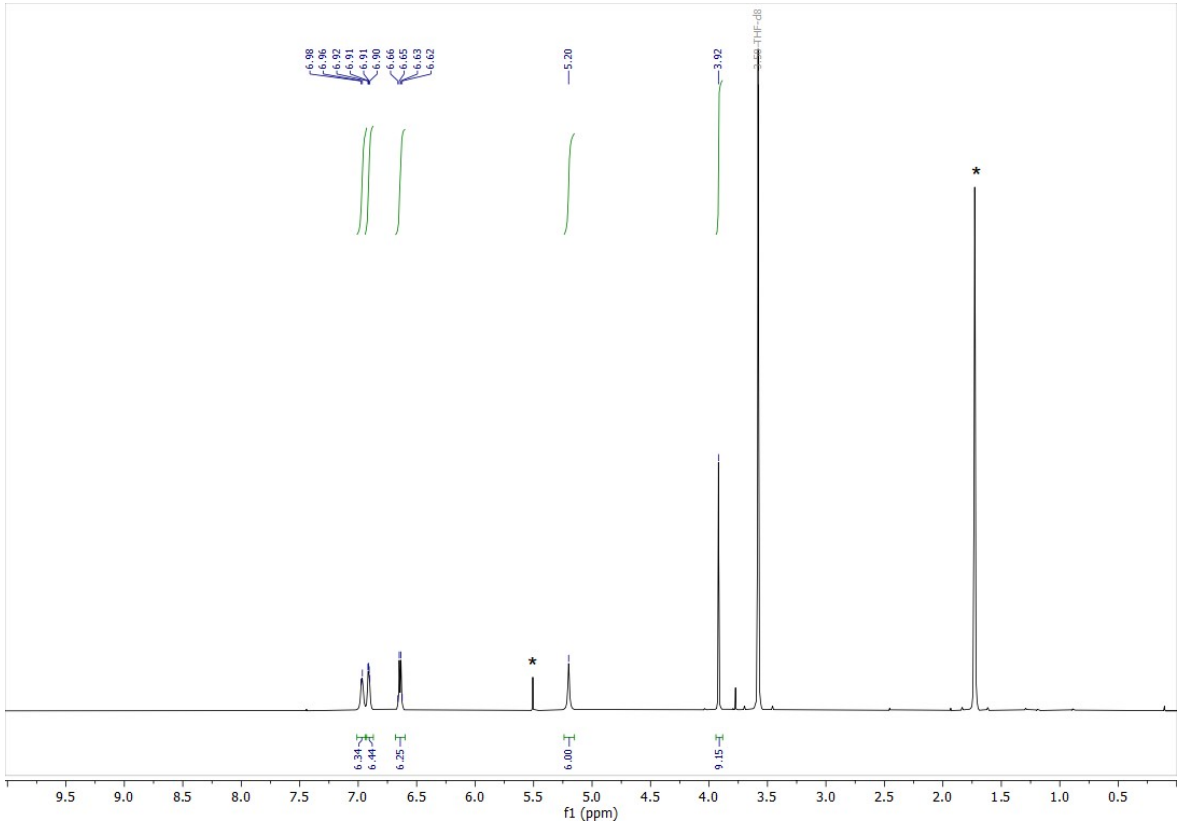

Figure S3.20. ^{1}H NMR spectrum (THF-d_8) of **NRos-6**

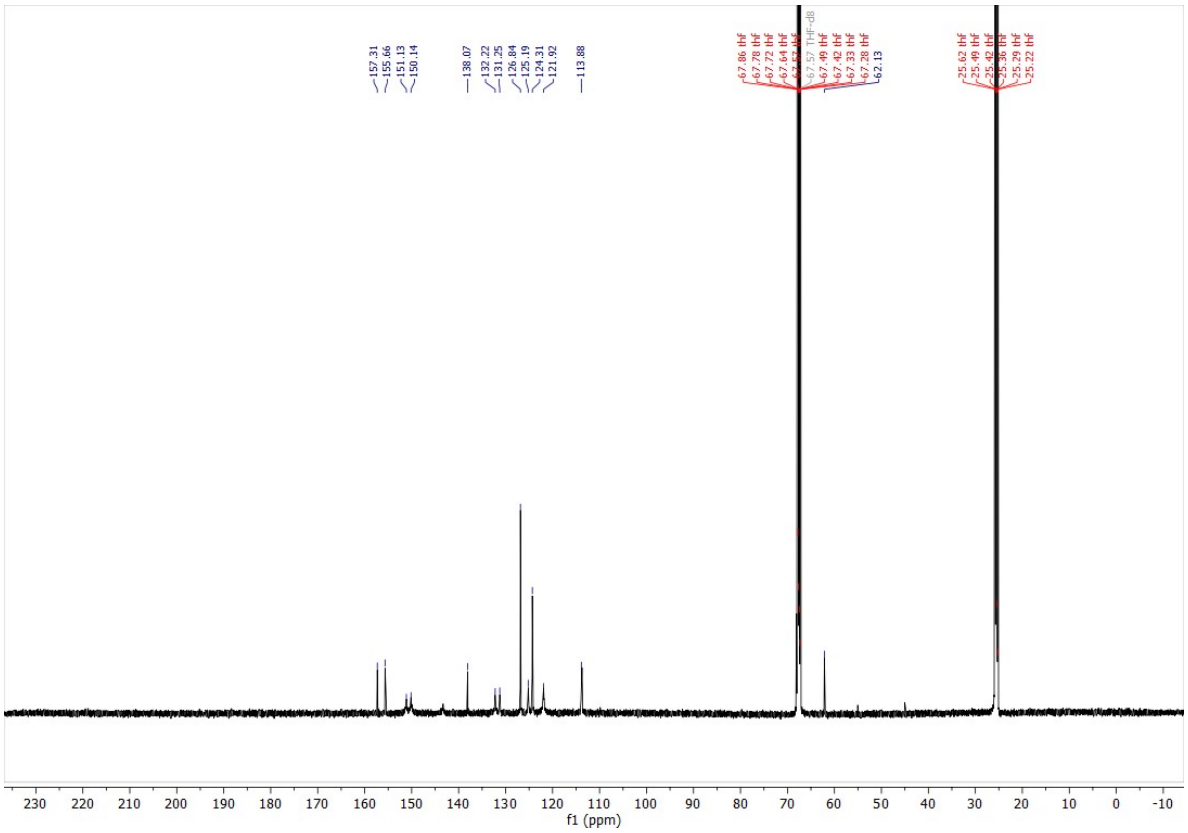

Figure S3.21. ^{13}C NMR spectrum (THF-d_8) of **NRos-6**

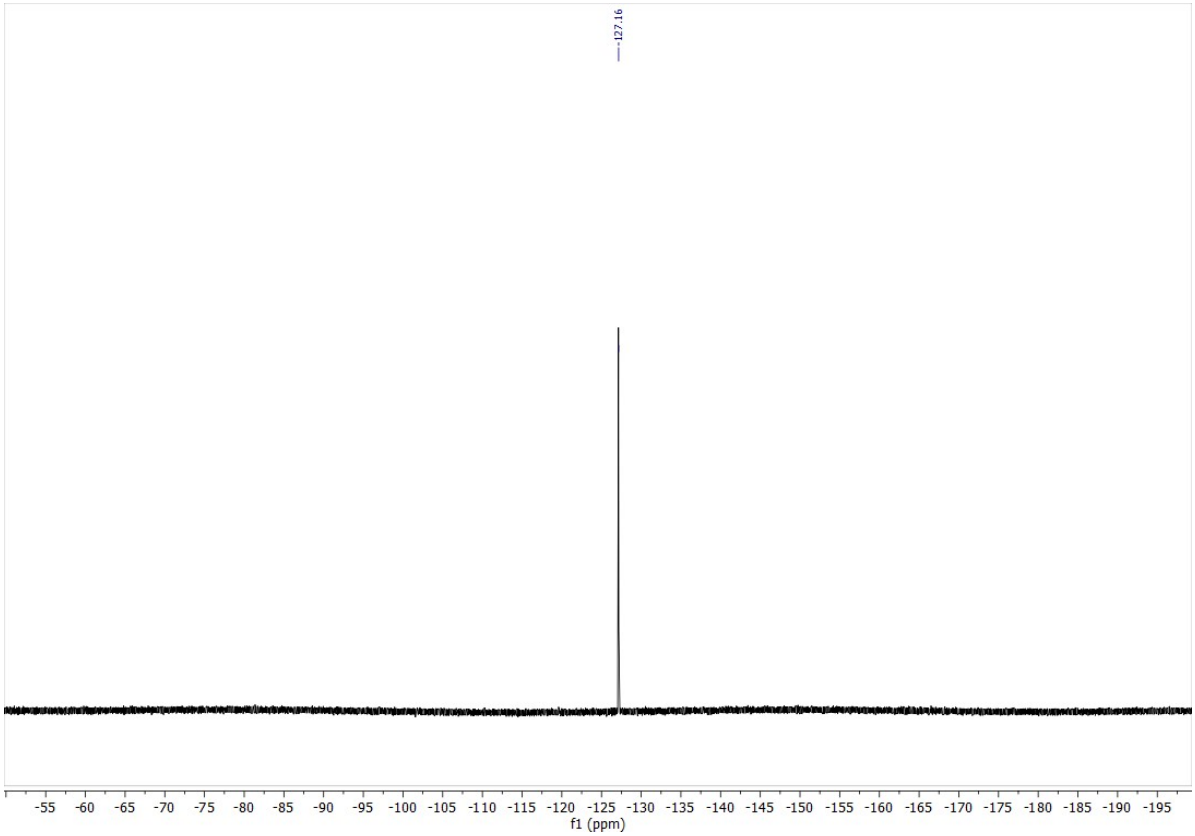

Figure S3.22. ^{19}F NMR spectrum (THF-d_8) of **NRos-6**

NRos-7

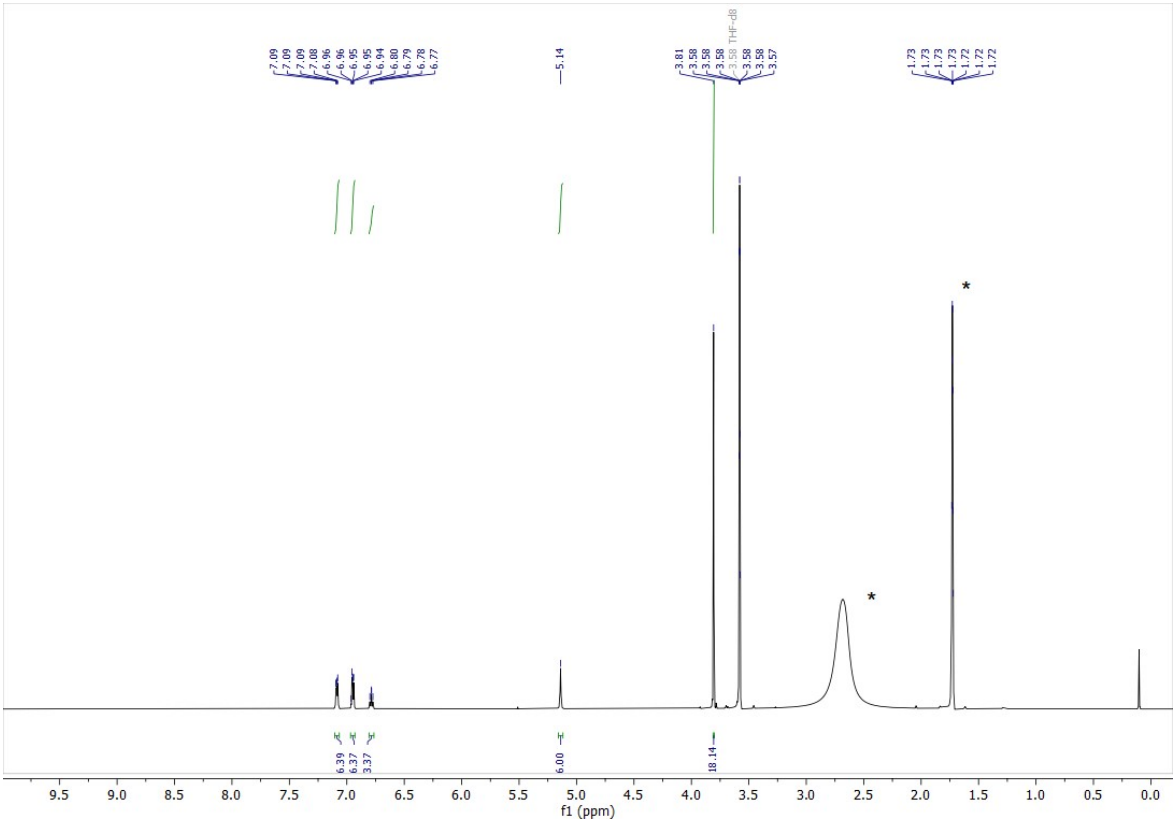

Figure S3.23. ^{1}H NMR spectrum (THF-d_8) of **NRos-7**

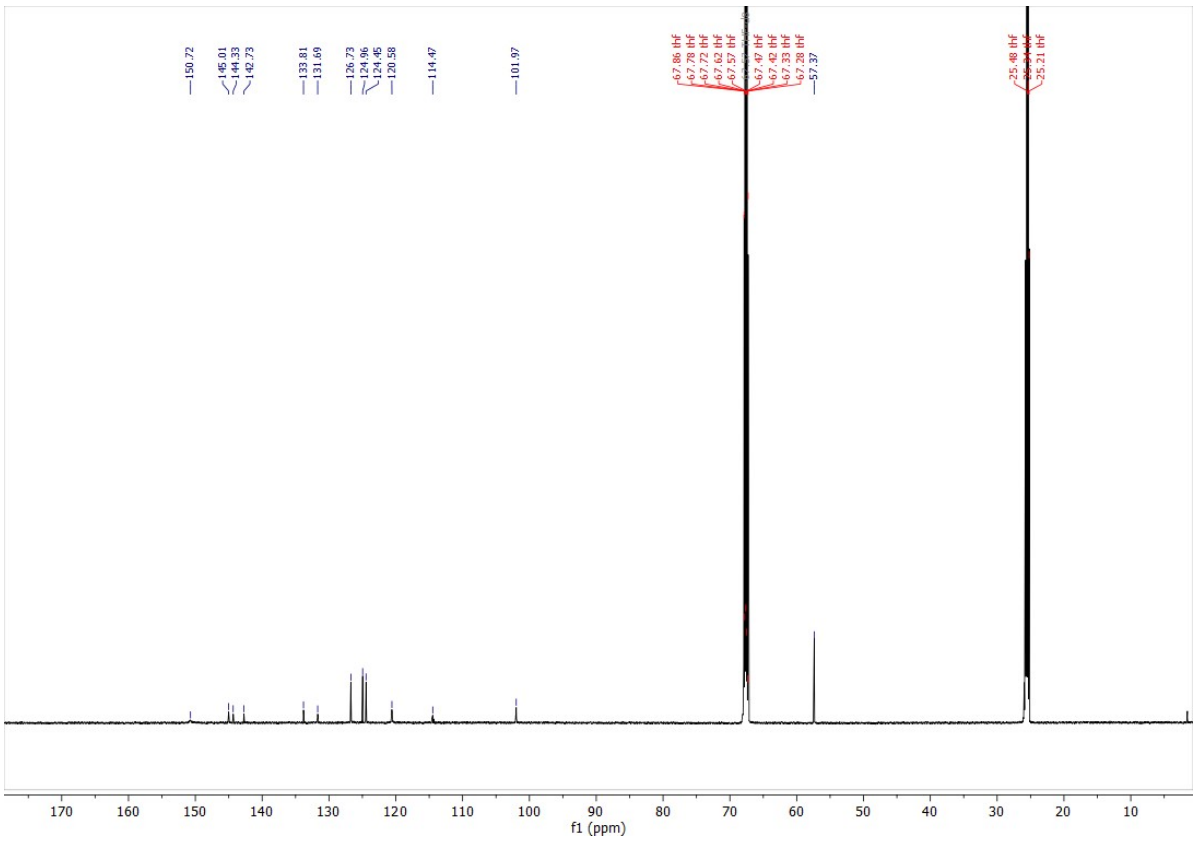

Figure S3.24. ^{13}C NMR spectrum (THF-d_8) of **NRos-7**

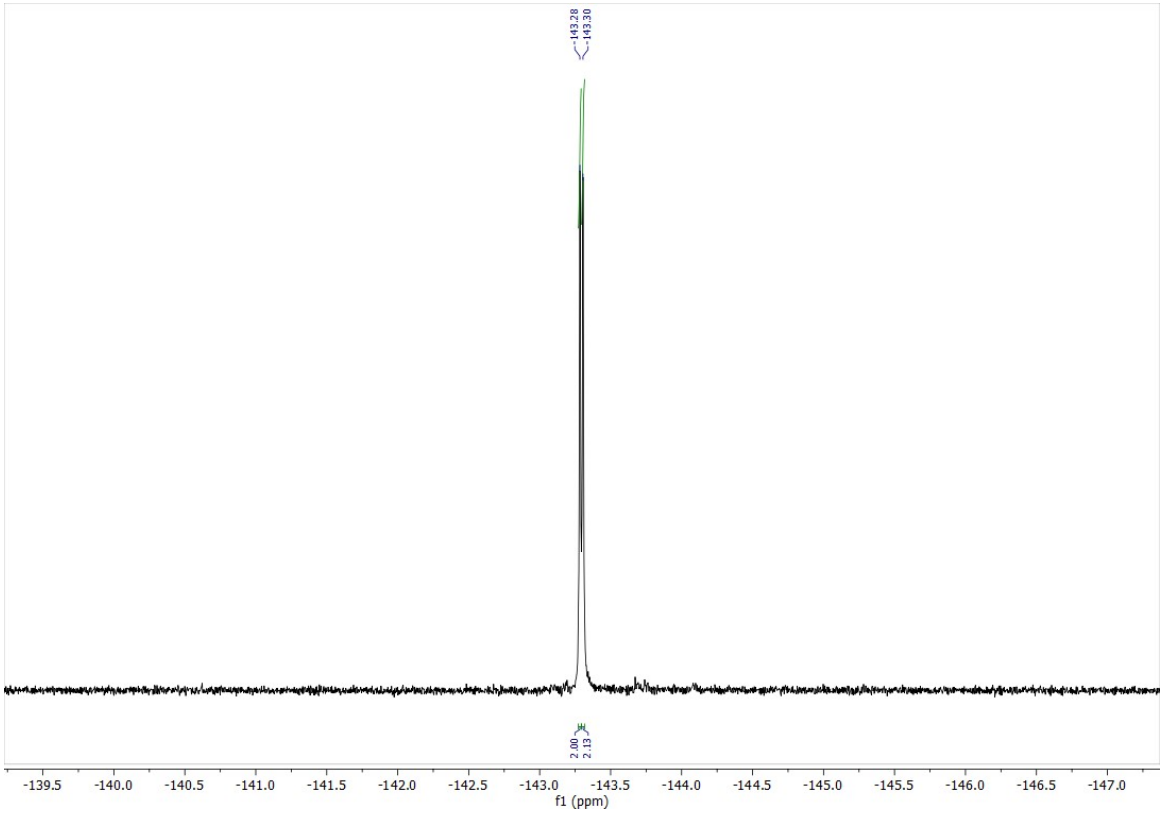

Figure S3.25. ^{19}F NMR spectrum (THF-d_8) of **NRos-7**

NRos-8

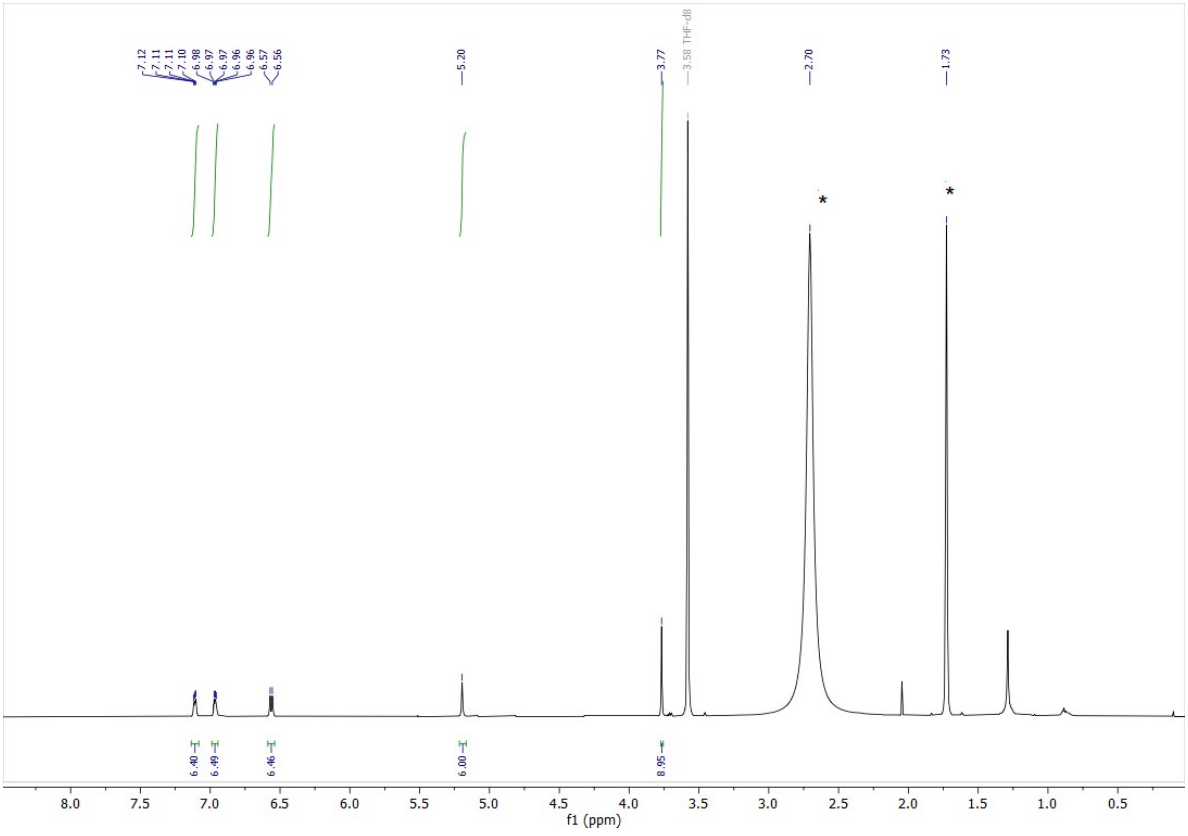

Figure S3.26. ^{1}H NMR spectrum (THF-d_8) of **NRos-8**

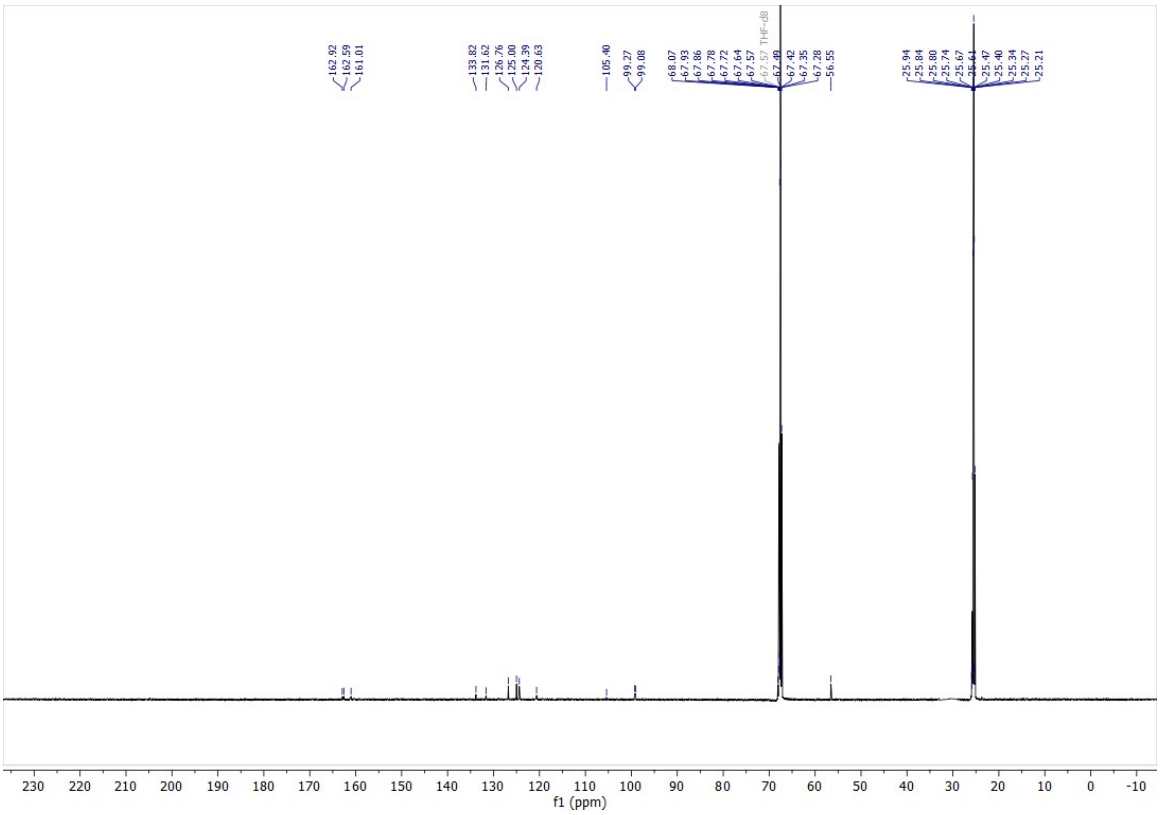

Figure S3.27. ^{13}C NMR spectrum (THF-d_8) of **NRos-8**

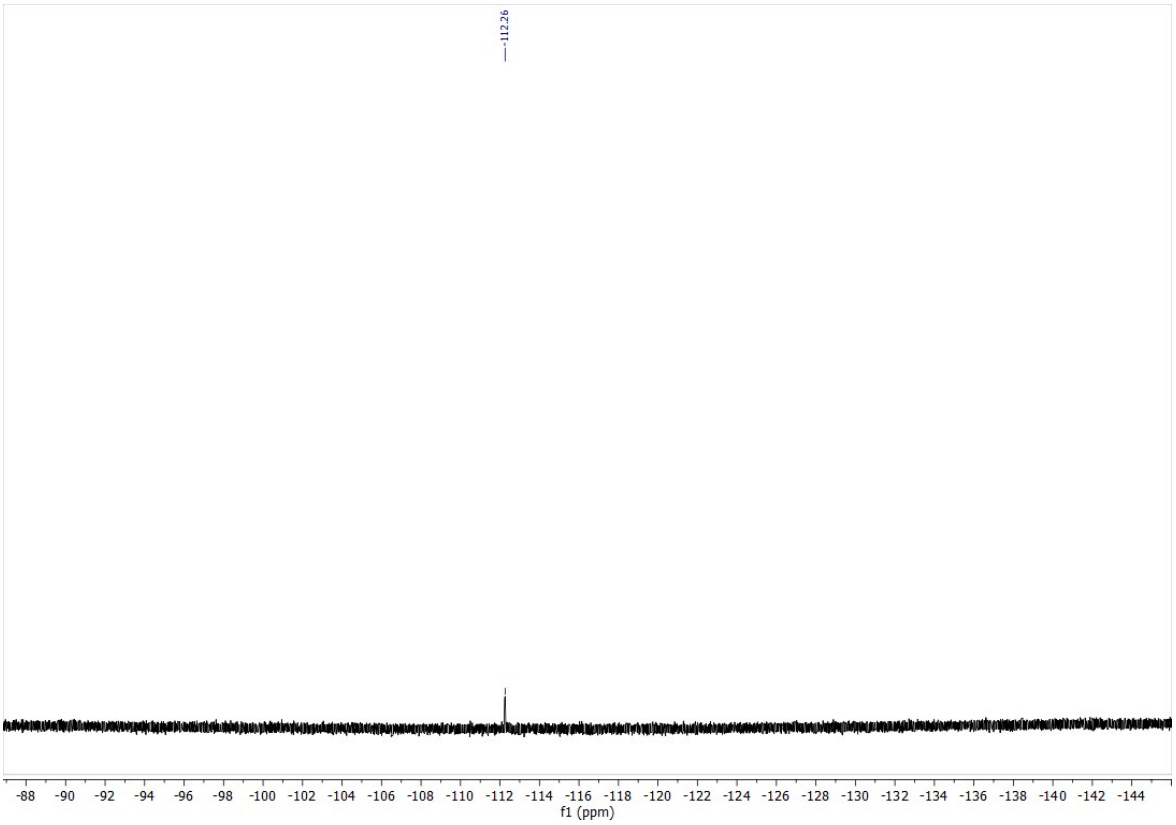

Figure S3.28. ^{19}F NMR spectrum (THF-d_8) of **NRos-8**

4. Mass Spectra

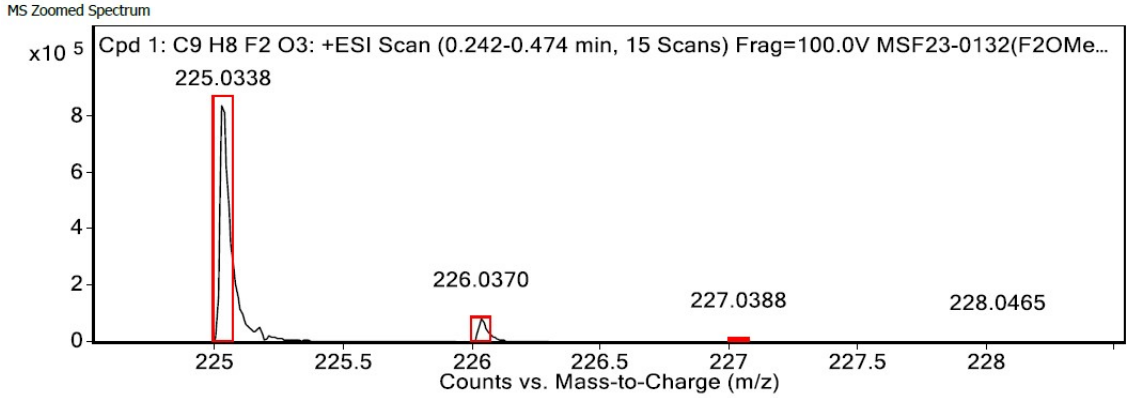

MS Spectrum Peak List

Obs. m/z	Calc. m/z	Charge	Abundance	Formula	Ion Species	Tgt Mass Error (ppm)
225.0338	225.0334	1	868627	C9H8F2O3	(M+Na)+	-2.1
226.0370	226.0368	1	83036	C9H8F2O3	(M+Na)+	-0.88
227.0388	227.0387	1	10190	C9H8F2O3	(M+Na)+	-0.38
228.0465	228.0414	1	1055	C9H8F2O3	(M+Na)+	-22.14
229.0698	229.0438	1	3582	C9H8F2O3	(M+Na)+	-113.71

--- End Of Report ---

Figure S4.1. HRMS of **2,6-difluoro-3,5-dimethoxybenaldehyde** (ESI-TOF, pos. mode, acetonitrile)

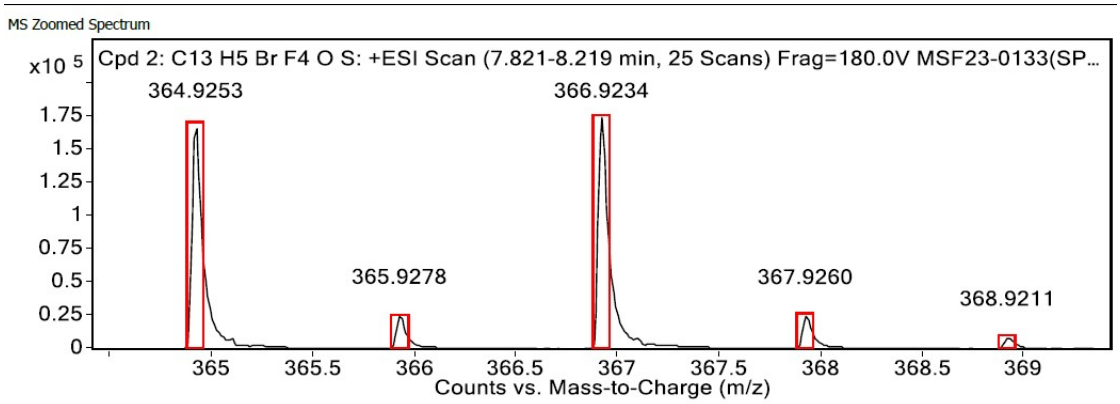

MS Spectrum Peak List

Obs. m/z	Calc. m/z	Charge	Abundance	Formula	Ion Species	Tgt Mass Error (ppm)
364.9253	364.9253	1	167559	C13H5BrF4OS	(M+H)+	0.11
365.9278	365.9285	1	25493	C13H5BrF4OS	(M+H)+	1.87
366.9234	366.9233	1	174318	C13H5BrF4OS	(M+H)+	-0.27
367.9260	367.9264	1	25242	C13H5BrF4OS	(M+H)+	1.08
368.9211	368.9214	1	9014	C13H5BrF4OS	(M+H)+	0.76

--- End Of Report ---

Figure S4.2. HRMS of **4-((4-bromophenyl)thio)-2,3,5,6-tetrafluorobenzaldehyde** (ESI-TOF, pos. mode, acetonitrile)

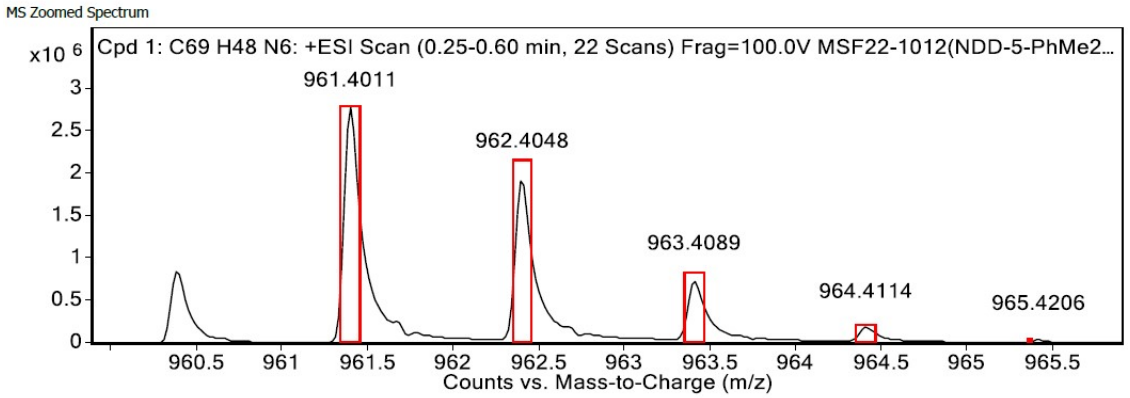

MS Spectrum Peak List

Obs. m/z	Calc. m/z	Charge	Abundance	Formula	Ion Species	Tgt Mass Error (ppm)
961.4011	961.4013	1	2786446	C69H48N6	(M+H)+	0.26
962.4048	962.4045	1	1945694	C69H48N6	(M+H)+	-0.26
963.4089	963.4077	1	738707	C69H48N6	(M+H)+	-1.2
964.4114	964.4109	1	168984	C69H48N6	(M+H)+	-0.56
965.4206	965.4141	1	28603	C69H48N6	(M+H)+	-6.69

--- End Of Report ---

Figure S4.3. HRMS of **NRos-1** (ESI-TOF, pos. mode, acetonitrile)

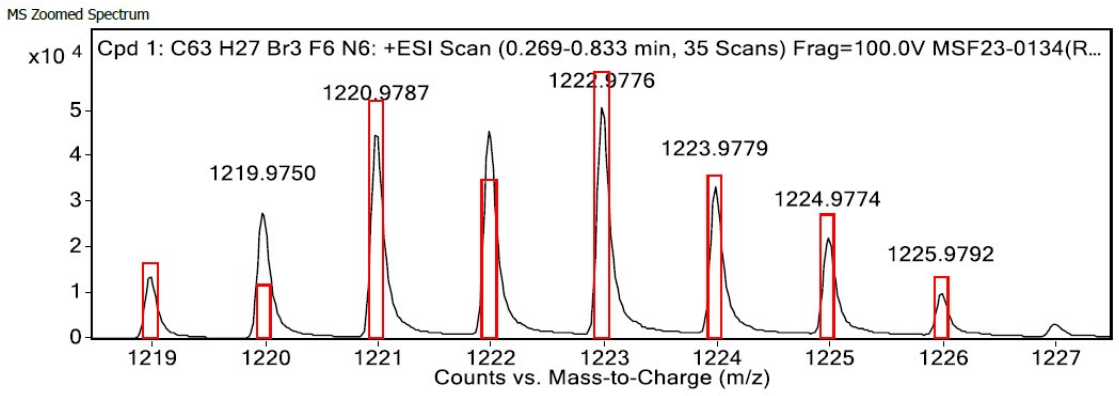

MS Spectrum Peak List

Obs. m/z	Calc. m/z	Charge	Abundance	Formula	Ion Species	Tgt Mass Error (ppm)
676.9426			128172			
1218.9791	1218.9824	1	13886	C63H27Br3F6N6	(M+H)+	2.69
1220.9787	1220.9810	1	45610	C63H27Br3F6N6	(M+H)+	1.91
1221.9769	1221.9838	1	46043	C63H27Br3F6N6	(M+H)+	5.66
1222.9776	1222.9801	1	51022	C63H27Br3F6N6	(M+H)+	1.99

--- End Of Report ---

Figure S4.4. HRMS of **NRos-3** (ESI-TOF, pos. mode, acetonitrile)

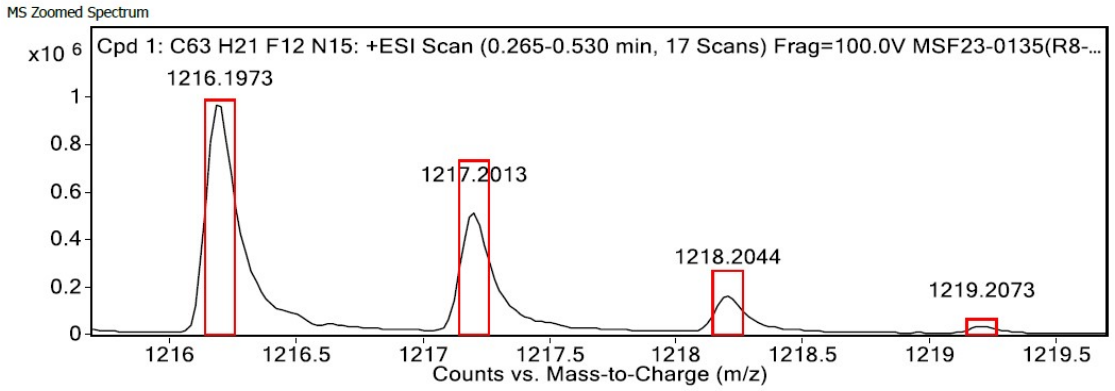

MS Spectrum Peak List

Obs. m/z	Calc. m/z	Charge	Abundance	Formula	Ion Species	Tgt Mass Error (ppm)
1216.1973	1216.1986	1	987391	C63H21F12N15	(M+H)+	1.01
1217.2013	1217.2014	1	517548	C63H21F12N15	(M+H)+	0.11
1218.2044	1218.2043	1	171030	C63H21F12N15	(M+H)+	-0.03
1219.2073	1219.2072	1	30602	C63H21F12N15	(M+H)+	-0.04
1220.2077	1220.2101	1	5459	C63H21F12N15	(M+H)+	1.99

--- End Of Report ---

Figure S4.9. HRMS of **NRos-4** (ESI-TOF, pos. mode, acetonitrile)

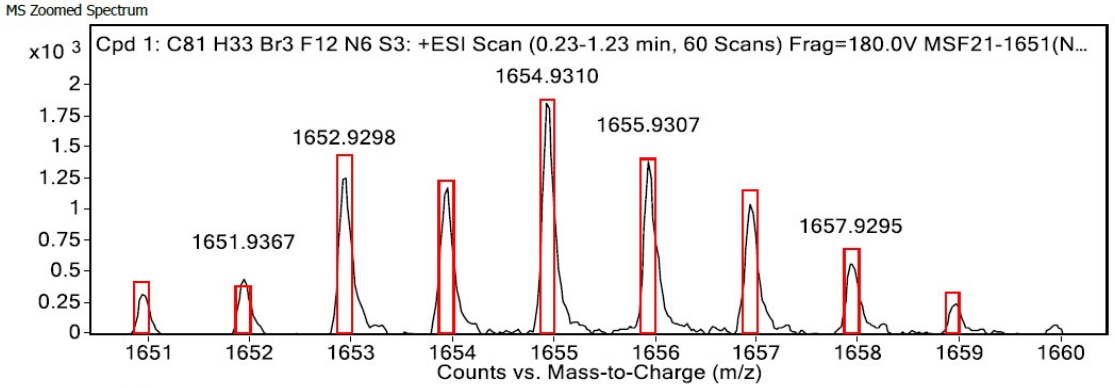

MS Spectrum Peak List

Obs. m/z	Calc. m/z	Charge	Abundance	Formula	Ion Species	Tgt Mass Error (ppm)
505.2004			8442			
1650.9456	1650.9360	1	327	C81H33Br3F12N6S3	(M+H)+	-5.82
1651.9367	1651.9391	1	443	C81H33Br3F12N6S3	(M+H)+	1.5
1652.9298	1652.9349	1	1284	C81H33Br3F12N6S3	(M+H)+	3.05
1653.9310	1653.9373	1	1189	C81H33Br3F12N6S3	(M+H)+	3.86
1654.9310	1654.9341	1	1882	C81H33Br3F12N6S3	(M+H)+	1.91
1655.9307	1655.9358	1	1385	C81H33Br3F12N6S3	(M+H)+	3.07
1656.9315	1656.9340	1	1050	C81H33Br3F12N6S3	(M+H)+	1.51
1657.9295	1657.9347	1	571	C81H33Br3F12N6S3	(M+H)+	3.1
1658.9427	1658.9347	1	254	C81H33Br3F12N6S3	(M+H)+	-4.82

--- End Of Report ---

Figure S4.8. HRMS of **NRos-5** (ESI-TOF, pos. mode, acetonitrile)

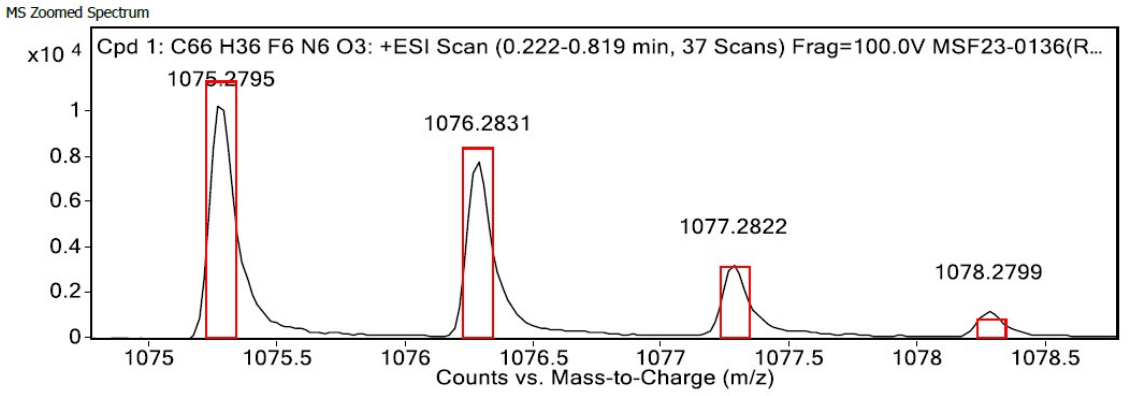

MS Spectrum Peak List

Obs. m/z	Calc. m/z	Charge	Abundance	Formula	Ion Species	Tgt Mass Error (ppm)
405.2801			18028			
1075.2795	1075.2826	1	10445	C66H36F6N6O3	(M+H)+	2.85
1076.2831	1076.2858	1	7807	C66H36F6N6O3	(M+H)+	2.44
1077.2822	1077.2889	1	3253	C66H36F6N6O3	(M+H)+	6.26
1078.2799	1078.2920	1	1239	C66H36F6N6O3	(M+H)+	11.22

--- End Of Report ---

Figure S4.6. HRMS of **NRos-6** (ESI-TOF, pos. mode, acetonitrile)

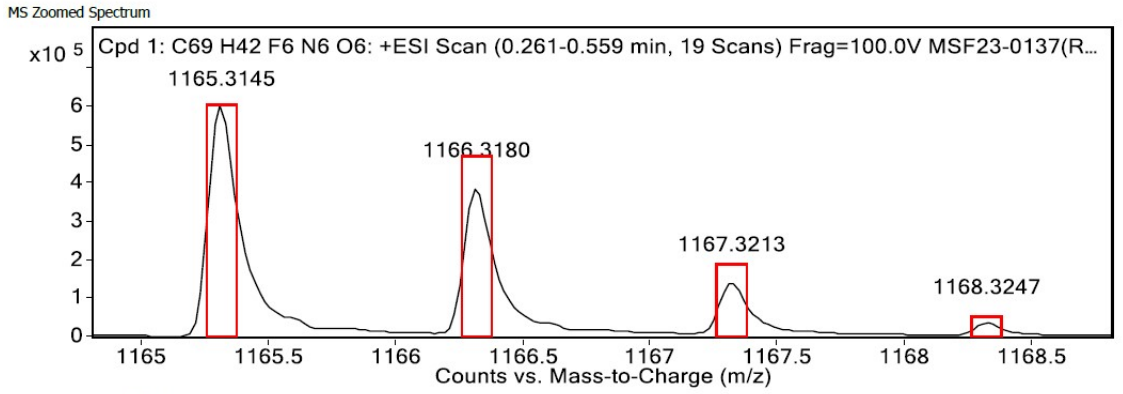

MS Spectrum Peak List

Obs. m/z	Calc. m/z	Charge	Abundance	Formula	Ion Species	Tgt Mass Error (ppm)
1165.3145	1165.3143	1	603884	C69H42F6N6O6	(M+H)+	-0.2
1166.3180	1166.3175	1	388211	C69H42F6N6O6	(M+H)+	-0.48
1167.3213	1167.3206	1	142759	C69H42F6N6O6	(M+H)+	-0.62
1168.3247	1168.3236	1	31616	C69H42F6N6O6	(M+H)+	-0.91
1169.3281	1169.3266	1	6047	C69H42F6N6O6	(M+H)+	-1.31

--- End Of Report ---

Figure S4.7. HRMS of **NRos-7** (ESI-TOF, pos. mode, acetonitrile)

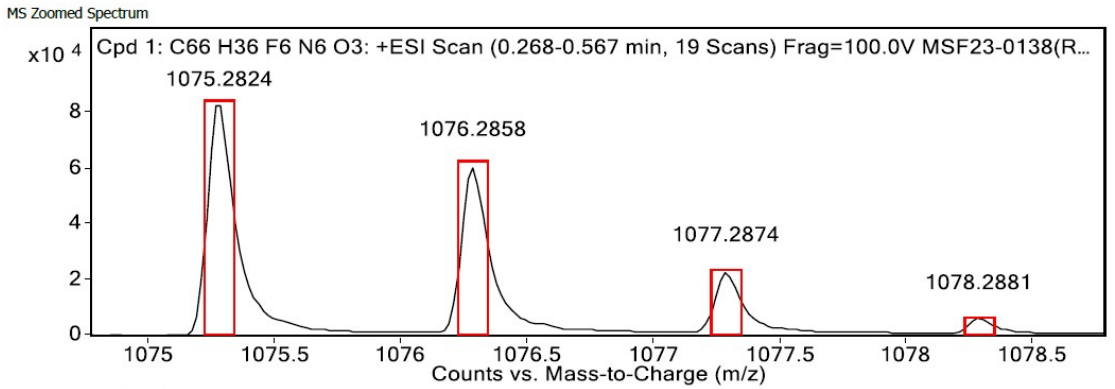

MS Spectrum Peak List

Obs. m/z	Calc. m/z	Charge	Abundance	Formula	Ion Species	Tgt Mass Error (ppm)
1075.2824	1075.2826	1	84141	C66H36F6N6O3	(M+H)+	0.2
1076.2858	1076.2858	1	60623	C66H36F6N6O3	(M+H)+	0.01
1077.2874	1077.2889	1	22685	C66H36F6N6O3	(M+H)+	1.41
1078.2881	1078.2920	1	5468	C66H36F6N6O3	(M+H)+	3.58
1079.2815	1079.2950	1	1345	C66H36F6N6O3	(M+H)+	12.58

--- End Of Report ---

Figure S4.5. HRMS of **NRos-8** (ESI-TOF, pos. mode, acetonitrile)

5. UV-vis Spectra

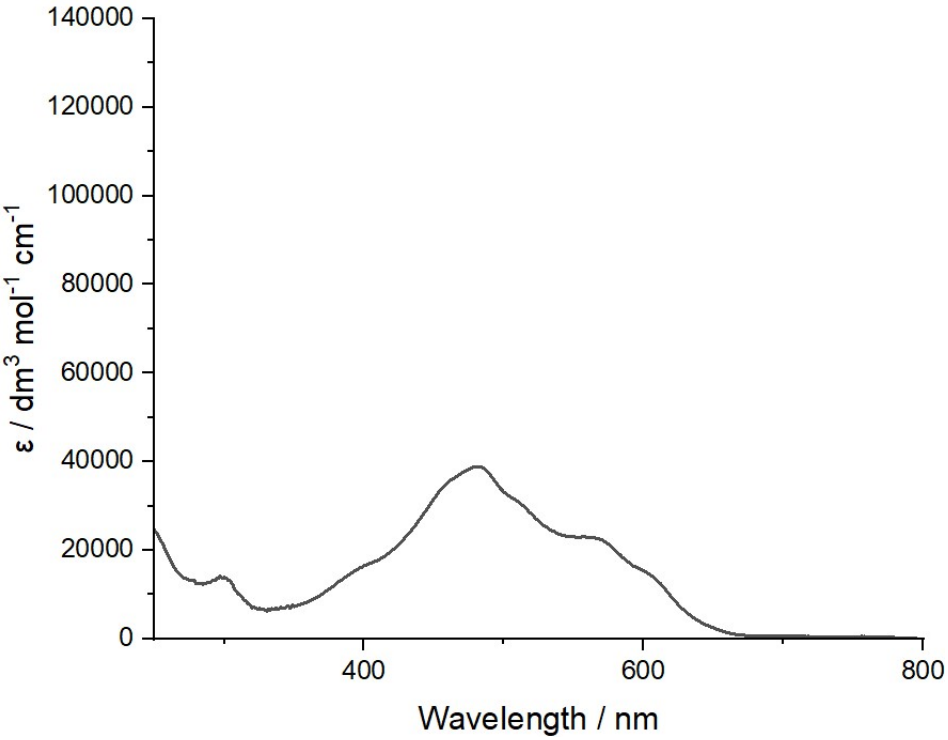

Figure S5.1. UV-vis absorption spectrum of **NRos-1** (in CH_2Cl_2).

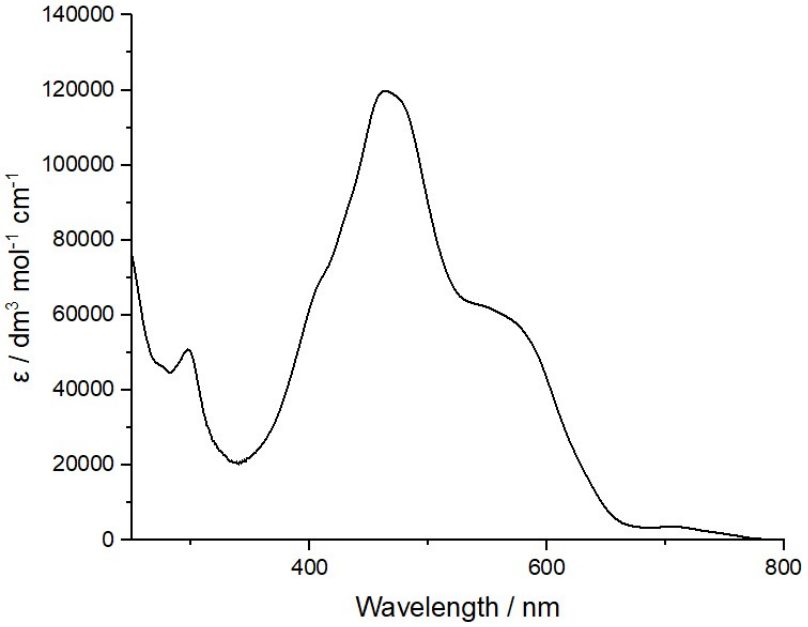

Figure S5.2. UV-vis absorption spectrum of of **NRos-2** (in CH_2Cl_2).

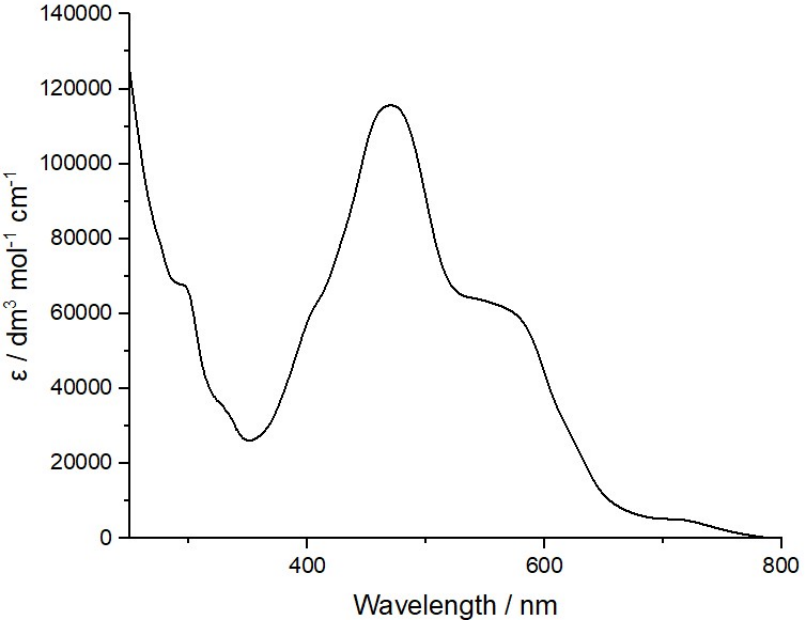

Figure S5.3. UV-vis absorption spectrum of of **NRos-3** (in CH_2Cl_2).

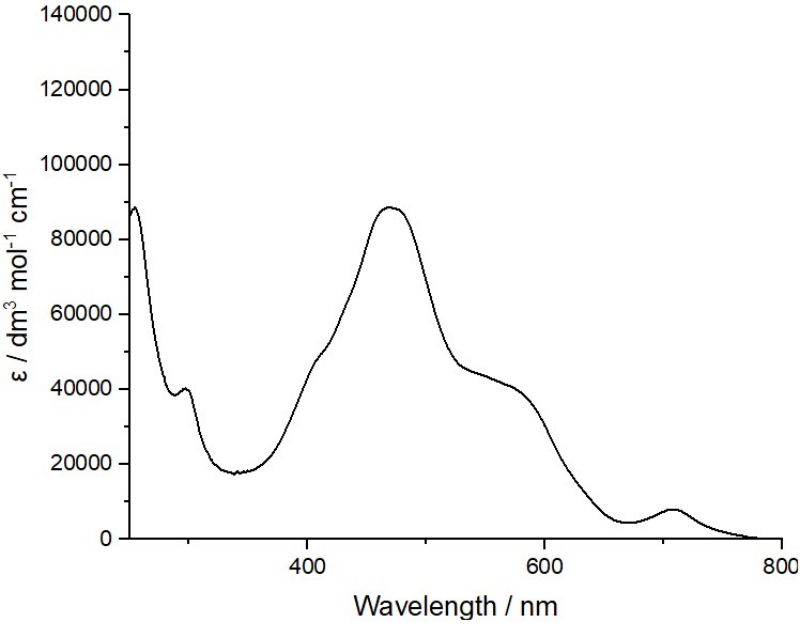

Figure S5.4. UV-vis absorption spectrum of **NRos-4** (in CH_2Cl_2).

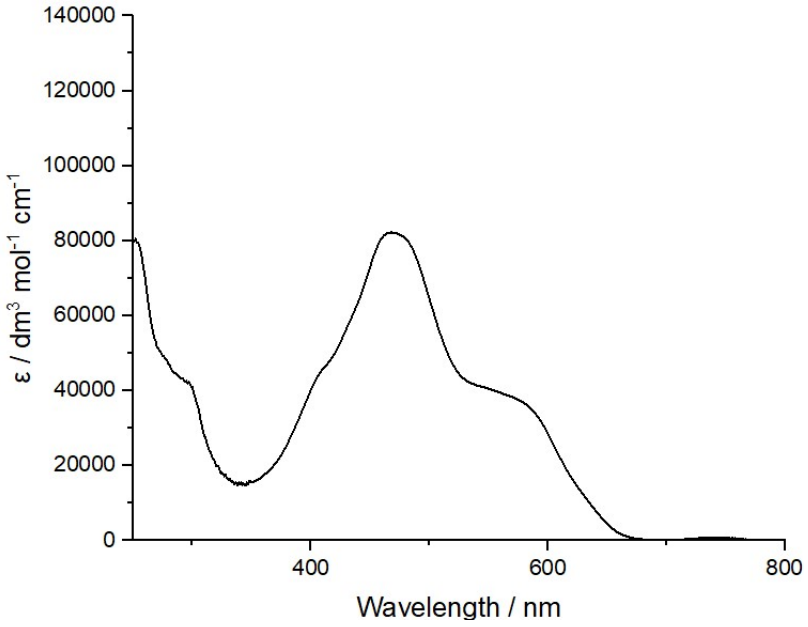

Figure S5.5. UV-vis absorption spectrum of **NRos-5** (in CH_2Cl_2).

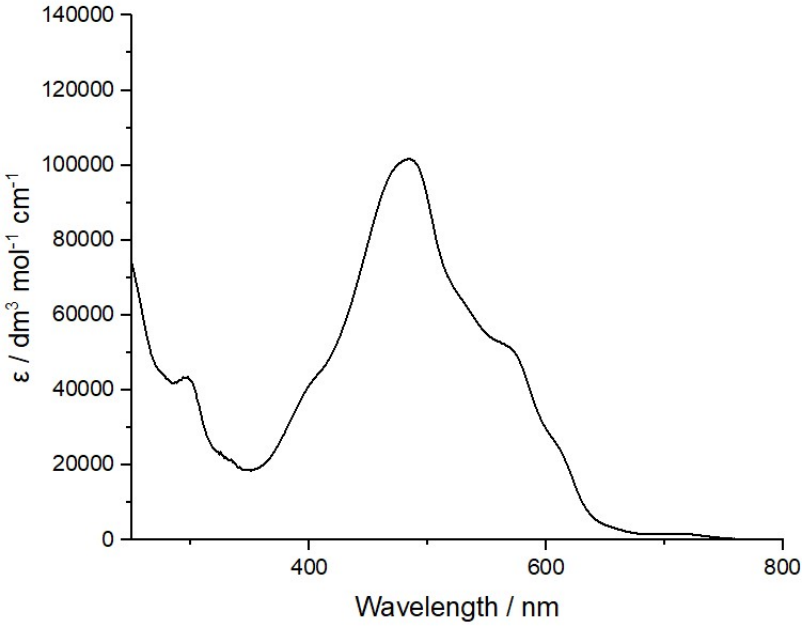

Figure S5.6. UV-vis absorption spectrum of **NRos-6** (in CH_2Cl_2).

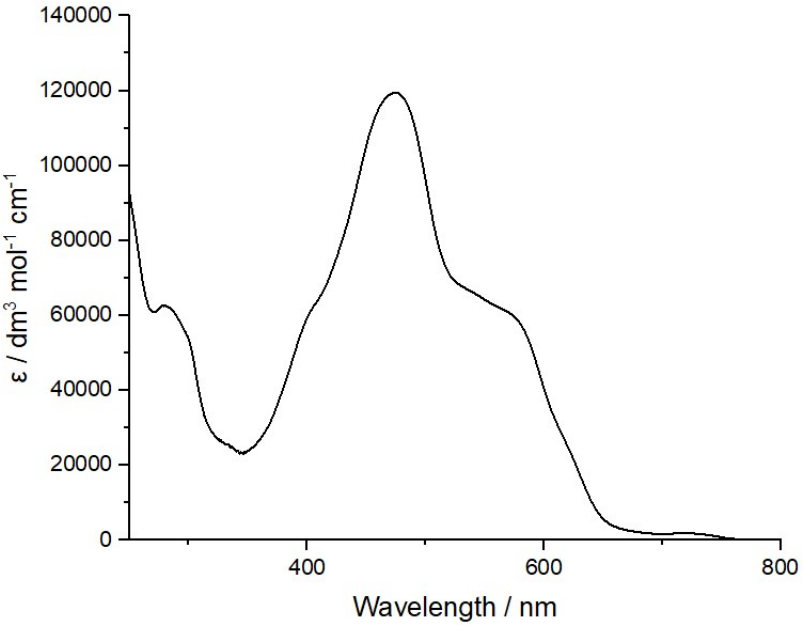

Figure S5.7. UV-vis absorption spectrum of **NRos-7** (in CH_2Cl_2).

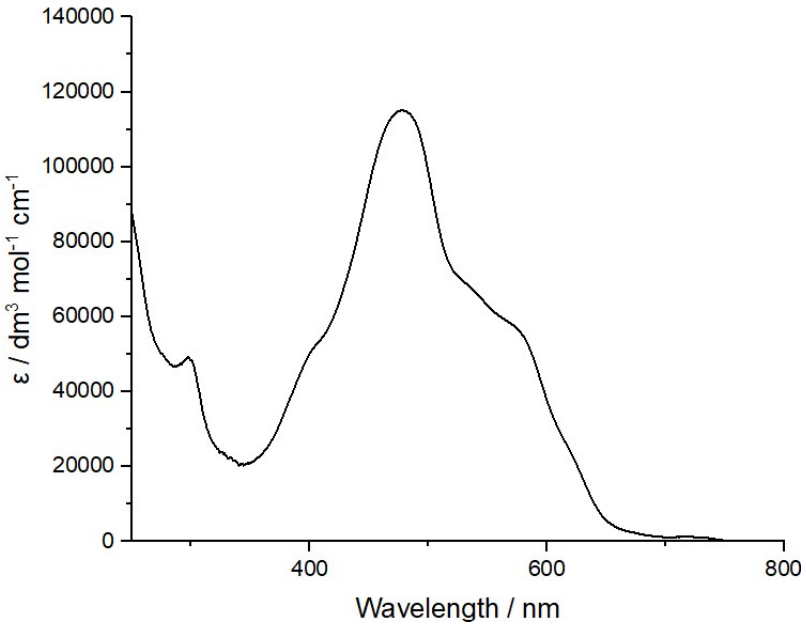

Figure S5.8. UV-vis absorption spectrum of **NRos-8** (in CH_2Cl_2).

6. Electrochemistry

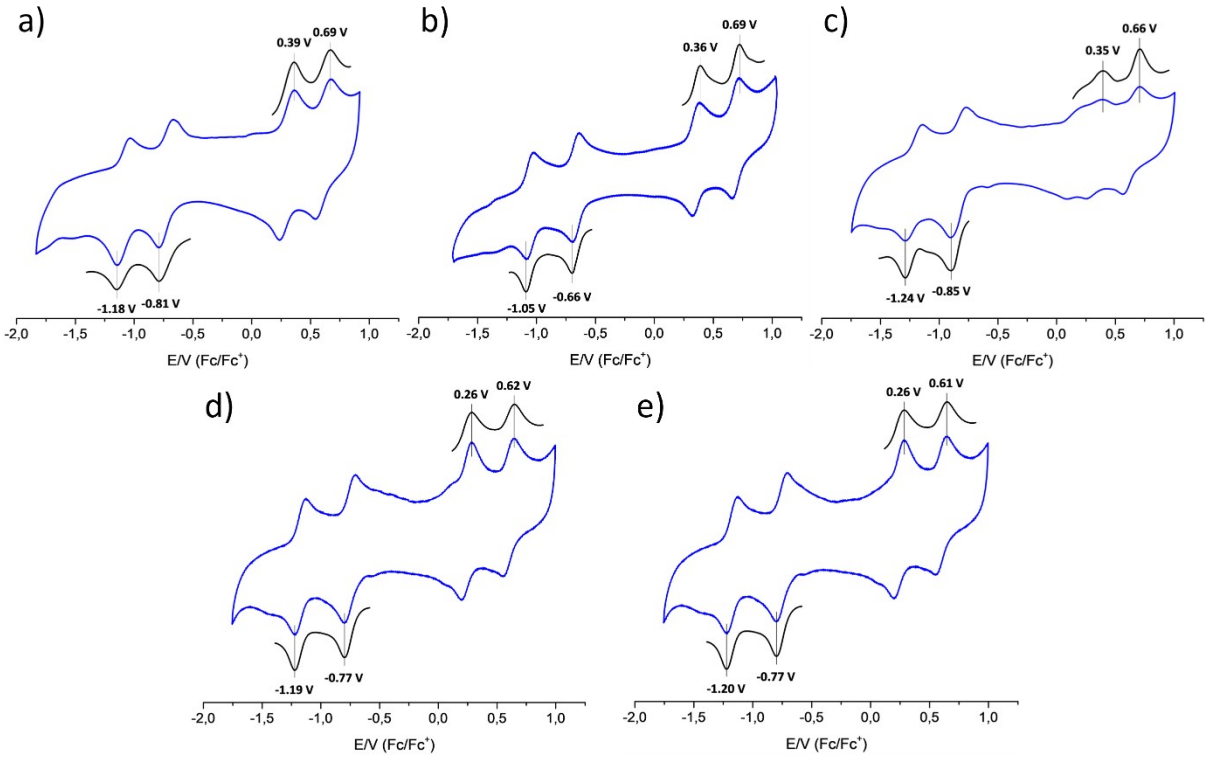

Figure S6.1. Cyclic (closed curves) and differential-pulse voltammograms (open graphs) of **NRos-2** (a), **NRos-3** (b), **NRos-6** (c), **NRos-7** (d) and **NRos-8** (e) recorded in CH_2Cl_2 at room temperature using Bu_4NPF_6 as the electrolyte.

7. Computational studies

All reported structures were optimized at the DFT level using the B3LYP[5] functional. The standard 6-31G(d,p) basis set was used for all atoms considered. Analytical harmonic frequencies were computed at the same level of theory to confirm the nature of the stationary points. All of the calculations were carried out by the methods implemented in the Gaussian 16 package.[6] TD-DFT calculations were carried out at the CAM-B3LYP/6-31+G(d,p) level of theory. For the mechanistic studies, the reported energy values correspond to the Gibbs Free (G) energies. Transition state geometries were connected with reactants and products via Intrinsic Reaction Coordinate (IRC) calculations. Solvent (CH_2Cl_2) effects were also considered through the Polarizable Continuum Model (PCM).

TD-DFT calculations

Excited state	Energy (nm)	*f*[a]	Orbitals[b] (coefficient)
S_1	1006	0.0000	H→L (69%)
S_2	541	0.0789	H-3→L+2 (11%)
			H-2→L+2 (12%)
			H-1→L (64%)
			H-1→L+1 (12%)
S_3	541	0.0789	H-3→L (11%)
			H-2→L (64%)
			H-2→L+1 (12%)
			H-1→L+2 (12%)
S_4	478	0.0000	H-3→L (57%)
			H-2→L+1 (15%)
			H-2→L+2 (22%)
			H-1→L+1 (22%)
			H-1→L+2 (15%)
S_5	436	1.1656	H-1→L (13%)
			H→L+1 (67%)
S_6	436	1.1656	H-2→L (13%)
			H→L+2 (67%)

Table S7.1. Selected transition properties of **NRos-2** calculated at the CAM-B3LYP/6-31+G(d,p) level of theory. [a]Oscillator strength. [b]MOs involved in the transitions (H and L denoting HOMO and LUMO).

Excited state	Energy (nm)	*f*[a]	Orbitals[b] (coefficient)
S_1	1088	0.0000	H→L (69%)
S_2	532	0.0889	H-3→L+1 (14%)
			H-2→L (63%)
S_3	532	0.0889	H-3→L+2 (14%)
			H-2→L (13%)
			H-2→L+1 (12%)
			H-1→L (63%)
S_4	471	0.0000	H-3→L (56%)
			H-2→L+1 (21%)
			H-2→L+2 (16%)
			H-1→L+1 (16%)
			H-1→L+2 (21%)
S_5	435	1.2324	H→L+1 (67%)

S_6	435	1.2324	H→L+2 (67%)

Table S7.2. Selected transition properties of **NRos-3** calculated at the CAM-B3LYP/6-31+G(d,p) level of theory. [a]Oscillator strength. [b]MOs involved in the transitions (H and L denoting HOMO and LUMO).

Excited state	Energy (nm)	*f*[a]	Orbitals[b] (coefficient)
S_1	1040	0.0000	H→L (69%)
S_2	519	0.1091	H-3→L+1 (13%)
			H-2→L (53%)
			H-2→L+2 (11%)
			H-1→L (38%)
			H-1→L+1 (11%)
S_3	519	0.1091	H-3→L+2 (13%)
			H-2→L (38%)
			H-2→L+1 (11%)
			H-1→L (53%)
			H-1→L+2 (11%)
S_4	463	0.0000	H-3→L (57%)
			H-2→L+1 (25%)
			H-1→L+2 (25%)
S_5	431	1.3314	H-2→L (11%)
			H→L+1 (67%)
S_6	430	1.3319	H-1→L (11%)
			H→L+2 (67%)

Table S7.3. Selected transition properties of **NRos-6** calculated at the CAM-B3LYP/6-31+G(d,p) level of theory. [a]Oscillator strength. [b]MOs involved in the transitions (H and L denoting HOMO and LUMO).

Excited state	Energy (nm)	*f*[a]	Orbitals[b] (coefficient)
S_1	1070	0.0000	H→L (69%)
S	523	0.0942	H-3→L+2 (14%)
			H-2→L (63%)
			H-2→L+2 (11%)
			H-1→L (14%)
			H-1→L+2 (11%)
			H→L+1 (10%)
S_3	523	0.0942	H-3→L+2 (14%)
			H-2→L (14%)

			H-2→L+1 (11%)
			H-1→L (63%)
			H-1→L+2 (11%)
			H→L+2 (10%)
S_4	463	0.0000	H-3→L (56%)
			H-2→L+1 (26%)
			H-1→L+2 (26%)
S_5	434	1.2517	H-2→L (11%)
			H→L+1 (67%)
S_6	434	1.2528	H-1→L (11%)
			H→L+2 (67%)

Table S7.4. Selected transition properties of **NRos-7** calculated at the CAM-B3LYP/6-31+G(d,p) level of theory. [a]Oscillator strength. [b]MOs involved in the transitions (H and L denoting HOMO and LUMO).

Excited state	Energy (nm)	f[a]	Orbitals[b] (coefficient)
S_1	1070	0.0000	H→L (69%)
S_2	523	0.0991	H-3→L+2 (11%)
			H-2→L (22%)
			H-2→L+1 (12%)
			H-1→L (61%)
			H-1→L+2 (12%)
S_3	523	0.0990	H-3→L+1 (11%)
			H-2→L (61%)
			H-2→L+2 (12%)
			H-1→L (22%)
			H-1→L+1 (12%)
S_4	464	0.0000	H-3→L (56%)
			H-2→L+1 (27%)
			H-1→L+2 (27%)
S_5	434	1.2687	H-2→L (13%)
			H→L+1 (67%)
S_6	434	1.2687	H-1→L (13%)
			H→L+2 (67%)

Table S7.5. Selected transition properties of **NRos-8** calculated at the CAM-B3LYP/6-31+G(d,p) level of theory. [a]Oscillator strength. [b]MOs involved in the transitions (H and L denoting HOMO and LUMO).

8. Supporting References

[1] N. R. Babij, E. O. McCusker, G. T. Whiteker, B. Canturk, N. Choy, L. C. Creemer, C. V. D. Amicis, N. M. Hewlett, P. L. Johnson, J. A. Knobelsdorf, F. Li, B. A. Lorsbach, B. M. Nugent, S. J. Ryan, M. R. Smith and Q. Yang, *Org. Process Res. Dev*. 2016, **20**, 661.

[2] Roznyatovskiy, V., Lynch, V. and Sessler, J. L., *Org. Lett.* 2010*,* **12**, 4424–4427.

[3] Keana, J. F. W.,Cai, X. S., *J. Org. Chem.* 1990, **55**, 3640–3647.

[4] a) M. Ishida, S. J. Kim, C. Preihs, K. Ohkubo, J. M. Lim, B. S. Lee, J. S. Park, V. M. Lynch, V. V. Roznyatovskiy, T. Sarma, P. K. Panda, C. H. Lee, S. Fukuzumi, D. Kim and J. L. Sessler , *Nat. Chem.*, 2012, **5**, 15. b) D. Firmansyah, S. J. Hong, R. Dutta, Q. He, J. Bae, H. Jo, H. Kim, K. M. Ok, V. M. Lynch, H. R. Byon, J. L. Sessler and C. H. Lee, *Chem. Eur. J.*, 2019, **25**, 3525.

[5] a) C. Lee, W. Yang, R. G. Parr, *Phys. Rev. B* 1988, **37**, 785–789. b) A. D. Becke, *J. Chem. Phys.* 1993, **98**, 5648. c) W. Kohn, A. D. Becke, R. G. Parr, *J. Phys. Chem.* 1996, **100**, 12974–12980

[6] Gaussian 16, Revision C.01; Frisch, M. J.; Trucks, G. W.; Schlegel, H. B.; Scuseria, G. E.; Robb, M. A.; Cheeseman, J. R.; Scalmani, G.; Barone, V.; Petersson, G. A.; Nakatsuji, H.; Li, X.; Caricato, M.; Marenich, A. V.; Bloino, J.; Janesko, B. G.; Gomperts, R.; Mennucci, B.; Hratchian, H. P.; Ortiz, J. V.; Izmaylov, A. F.; Sonnenberg, J. L.; Williams-Young, D.; Ding, F.; Lipparini, F.; Egidi, F.; Goings, J.; Peng, B.; Petrone, A.; Henderson, T.; Ranasinghe, D.; Zakrzewski, V. G.; Gao, J.; Rega, N.; Zheng, G.; Liang, W.; Hada, M.; Ehara, M.; Toyota, K.; Fukuda, R.; Hasegawa, J.; Ishida, M.; Nakajima, T.; Honda, Y.; Kitao, O.; Nakai, H.; Vreven, T.; Throssell, K.; Montgomery, J. A., Jr.; Peralta, J. E.; Ogliaro, F.; Bearpark, M. J.; Heyd, J. J.; Brothers, E. N.; Kudin, K. N.; Staroverov, V. N.; Keith, T. A.; Kobayashi, R.; Normand, J.; Raghavachari, K.; Rendell, A. P.; Burant, J. C.; Iyengar, S. S.; Tomasi, J.; Cossi, M.; Millam, J. M.; Klene, M.; Adamo, C.; Cammi, R.; Ochterski, J. W.; Martin, R. L.; Morokuma, K.; Farkas, O.; Foresman, J. B.; Fox, D. J. Gaussian, Inc., Wallingford CT, 2016